Soil Science Society of America Journal

ORIGINAL ARTICLE

Fundamental Soil Science

Soil development and ancient Maya land use in the tropical karst landscape: Case of Busiljá, Chiapas, México

P. García-Ramírez¹ K. Guillén¹ S. Sedov² C. Golden³ S. Morell-Hart⁴ A. Scherer⁴ | T. Pi² | E. Solleiro-Rebolledo² | H. Dine⁴

Correspondence

P. García-Ramírez, Posgrado en Ciencias de la Tierra, Instituto de Geología, Universidad Nacional Autónoma de México, Ciudad Universitaria, 04510, México.

Email: arqueopams42@outlook.com

Assigned to Associate Editor Kyungsoo

Funding information

Social Sciences and Humanities Research Council of Canada, Grant/Award Number: 435-2019-0837; Alphawood Foundation of Chicago; National Science Foundation of the United States of America, Grant/Award Number: BCS 1917671; PAPIIT-DGAPA, Grant/Award Numbers: IN105819, IN108622; The Hitz Foundation; Consejo Nacional de Humanidades, Ciencia y Tecnología (CONAHCYT), Grant/Award Number: CF682138

Abstract

The soil mantle of the tropical karstic landscapes of Southern Mexico was shaped by specific processes of pedogenesis and long-term human impacts of ancient Maya agriculture. To understand the interaction between natural and human-induced soilforming processes in the calcareous mountains of Chiapas state, we studied soil toposequences around the Classic Maya site of Budsilhá and related them to the archaeological evidence of settlement and land-use distribution. Soil chemical analysis, micromorphological observations, and clay mineral identification were carried out in key soil profiles at the main geoforms. Limestone hills are occupied by shallow Rendolls which are usually perceived as incipient soils. However, high content of silicate clay composed of kaolinite and vermiculite and ferruginous clayey soil material observed at macro- and microscale backed the hypothesis that these soils were formed from the residues of thick Terra Rossa after their erosion. Swampy lowlands are occupied by thick clayey gleyic soils with clay mineral assemblages similar to those in the upland Rendolls. We suppose that the mineral matrix of the lowland soils is largely derived from the pedosediments of eroded upland Terra Rossa, which lost original ferruginous pigmentation and aggregation due to redoximorphic processes. Some wetland soils contain neoformed gypsum that is atypical for humid tropics; sulfidesulfate transformation under fluctuating redox conditions could promote gypsum synthesis. Ancient Maya land use was closely related to soil-geomorphic conditions: settlements with homegardens occupied calcareous hills, whereas the primary agricultural domain was developed on lowland soils after their drainage by artificial

Abbreviations: FWHM, full width at half maximum; HIV, hydroxy-interlayered vermiculite; LiDAR, light detection and ranging; MPERF, McMaster Paleoethnobotanical Research Facility; NCALM, National Center for Airborne Laser Mapping; PABC, Proyecto Arqueológico Busiljá-Chocoljá; UNAM, Universidad Nacional Autónoma de México; XRD, X-ray diffraction.

This is an open access article under the terms of the Creative Commons Attribution-NonCommercial-NoDerivs License, which permits use and distribution in any medium, provided the original work is properly cited, the use is non-commercial and no modifications or adaptations are made. © 2024 The Author(s). Soil Science Society of America Journal published by Wiley Periodicals LLC on behalf of Soil Science Society of America.

Soil Sci. Soc. Am. J. 2024;1-22.



¹Posgrado en Ciencias de la Tierra, Instituto de Geología, Universidad Nacional Autónoma de México, Ciudad Universitaria, México

²Instituto de Geología, Universidad Nacional Autónoma de México, Ciudad Universitaria, México

³Department of Anthropology, Brandeis University, Waltham, Massachusetts, USA

⁴Department of Anthropology, Brown University, Providence, Rhode Island, USA

1 | INTRODUCTION

From Southern Mexico's Isthmus of Tehuantepec eastward to northern Central America, Classic Maya society (c. AD 250–900) gave rise to an ancient agricultural economy with high efficiency and productivity developed in the humid tropics (e.g., Dunning et al., 2002; Fedick, 1996; Krause et al., 2021; Luzzadder-Beach et al., 2020; Morell Hart et al., 2023). A large part of this region is occupied by karstic geosystems formed in the sedimentary sequences dominated by calcareous rocks: limestones and dolomites (Espinasa-Pereña, 1990). Ancient agrosystems were developed within the karstic landscapes and adjusted to the specific characteristics of its soil mantle.

Pedogenesis on calcareous rocks affected by the karstification processes differs significantly from the "central image" of soil development in the humid tropics. Frequently, the soils are represented by shallow Rendzina type profiles (Rendolls), whereas deep strongly weathered soils—Oxisols and Ultisols—are usually formed on the silicate materials under humid tropical climate; on the other hand, much more developed soils enriched in silicate clay and iron oxides are also found on the limestones that often neighbor Rendzinas. These soils are frequently referred to as Terra Rossa and they are mostly red Alfisols. The origin of their parent material as well as their pedogenesis are still under debate (Durn, 2003; Durn et al., 1999; Priori et al., 2008; Yaalon, 1997). High pedodiversity of karstic soils provides both advantages and challenges for agricultural use.

Extensive research concerning the development, utilization, and transformation of the soil mantle in the platform karst landscapes of the Maya Lowlands in the Yucatan Peninsula has been carried out over the last several decades. The primary soil types have been characterized and their relationship with the geoforms and calcareous rock types has been established (Bautista et al., 2011; Bautista-Zuñiga et al., 2004). The detailed study of composition and structure of mineral soil matrix has been performed both in Rendzinas (Sedov et al., 2008) and Terra Rossa types of soils (Cabadas-Báez et al., 2010a), which has aided attempts to trace their origin and pedogenic transformation. Soil constraints for ancient Maya cultivation have been identified (Beach, 1998b) and evidence of soil degradation has been revealed (Beach et al., 2006). Short-distance variability of soil cover has been investigated in relation to the design of traditional Maya agrosystems (Fedick et al., 2008; Flores-Delgadillo et al., 2011). Hidden karstic erosion, soil piping, has been proposed as the main mechanism of soil loss in the Maya lowlands (Sedov et al., 2008), and pedosediments of the karstic pockets have been investigated as possible indicators of soil redeposition (Cabadas-Báez et al., 2010a; Solleiro

Core Ideas

- Ancient Maya land use was adjusted to pedodiversity and impacted soil development.
- Shallow upland Rendolls developed due to erosion of pre-existing red clayey soils.
- Depressions soils contain redeposited material from the uplands (clay mineralogy).
- Neoformed gypsum is uncommon in humid tropics as a result of redoximorphic processes.

et al., 2015). In addition to well-drained upland soils, the profiles of extensive flooded depressions have been investigated and a scenario of their use by ancient Maya people has been proposed (Leonard et al., 2019; Solleiro et al., 2015).

Much less is known about the soil mantle of the hilly karstic landscapes which comprise the northwestern part of the Maya region. Soilscapes of calcareous ridges which outline the upper Usumacinta River Valley, the location of many famous Maya sites, like Palenque, Piedras Negras, Yaxchilán, and Bonampak among others, are still poorly documented. Previous paleopedological and soil-archaeological research focused on the soil-sedimentary sequences of the alluvial terraces of the Usumacinta, to obtain paleoenvironmental records (Solís-Castillo et al., 2013, 2015) and show their possible relevance for ancient Maya population patterns (Liendo et al., 2014). Upland soils are less well documented. In the area of Piedras Negras, Guatemala, some data about soil resources for ancient Maya agriculture are available including estimated rates of pedogenesis and limited studies of cultivation indicators like phytoliths and stable carbon isotope composition of organic matter (Fernandez et al., 2005; Johnson et al., 2007). Only fragmentary information exists about a scant handful of profiles of the hilly karstic landscapes surrounding Mayan urban centers in Chiapas (Chávez-Herrerías, 2023).

To address these research gaps, we performed an interdisciplinary study of the soil mantle of the area surrounding the ancient Maya site of Budsilhá, Chiapas, to interpret the pedogenesis of its main constituents, understand how the ancient land use was tailored to soil diversity, and detect soil transformation due to human impact. We applied the catenary approach which has proven to be suitable for the pedoarchaeological investigations in Maya region (Beach, 1998a). During this research, some unexpected soil types and intriguing soil features were encountered, which required novel interpretation of their origin, (paleo)environmental significance, and role in the Maya cultural landscape.



FIGURE 1 Location of study area with some of the primary archaeological Maya sites.

1.1 | Geographical setting

Located in the Mexican state of Chiapas, near the border with Guatemala (Figure 1), our study area has been classified as tropical karst in faulted or folded mountains (Espinasa-Pereña, 1990).

The geology of this region is composed of limestones and shale-sandstone rocks folded in a NW-SE direction (INEGI, 1984a, 1984b). According to Servicio Geológico Mexicano (SGM, 2006a, 2006b), two formations are present in the area: the Tenejepa-Lacandon formation of limestone and the Lomut formation of limestone-sandstone, both dated from the Paleogene (SGM, 2006a, 2006b).

The climate of the area is warm humid with an average annual rainfall of 3413 mm, evapotranspiration of 1220 mm, and an average annual temperature of 24°C (CONAGUA, 2020).

Studies of land use and vegetation (INEGI, 2016) show a predominance of cultivated pasture in the valley area, where most of the study profiles are located, some patches of secondary shrub vegetation of high perennial forest to the south, and secondary arboreal vegetation of high perennial forest to the east, north, and southwest.

According to INEGI (2007a, 2007b), which follows the World Reference Base classification (IUSS Working Group WRB, 2015), the soils present in the area are primarily Luvisols, Leptosols, and Phaeozems, with chromic, humic, rendzic, and lithic qualifiers. In the valley zone, with thick

fine-textured sediments, deep well-developed Luvisols predominate. The area of mountains and hills is covered with Leptosols and Phaeozems.

1.2 | Cultural history

The cultural history of the area around the site of Budsilhá is intertwined with the development of the kingdoms of Palenque, Piedras Negras, Tonina, and La Mar from the Early Classic, 350–600 AD, to the Terminal Classic, 810–900 AD. The archaeological site of Budsilhá is located just northeast of the town of Nueva Esperanza Progresista, close to the Busiljá River, located 450 m to the south, is a significant tributary of the Usumacinta River that is the source of the site name. The first description of the site was published by Maler (1903), based on his explorations of the region a few years prior. Andrew Scherer and Charles Golden began research at Budsilhá more than a century later with the Proyecto Arqueológico Busiljá-Chocoljá (PABC) (Scherer & Golden, 2012), undertaking a more detailed description, mapping, and excavations efforts during 2012, 2013, and 2018, including excavations centered on the identification of probable agricultural areas associated with the site and residential groups (e.g., Dine, 2018b; Scherer et al., 2012).

From the work by the PABC (Scherer & Golden, 2012), it is known that the site dates to at least 600 AD, historical texts inscribed on stone monuments provide evidence of the

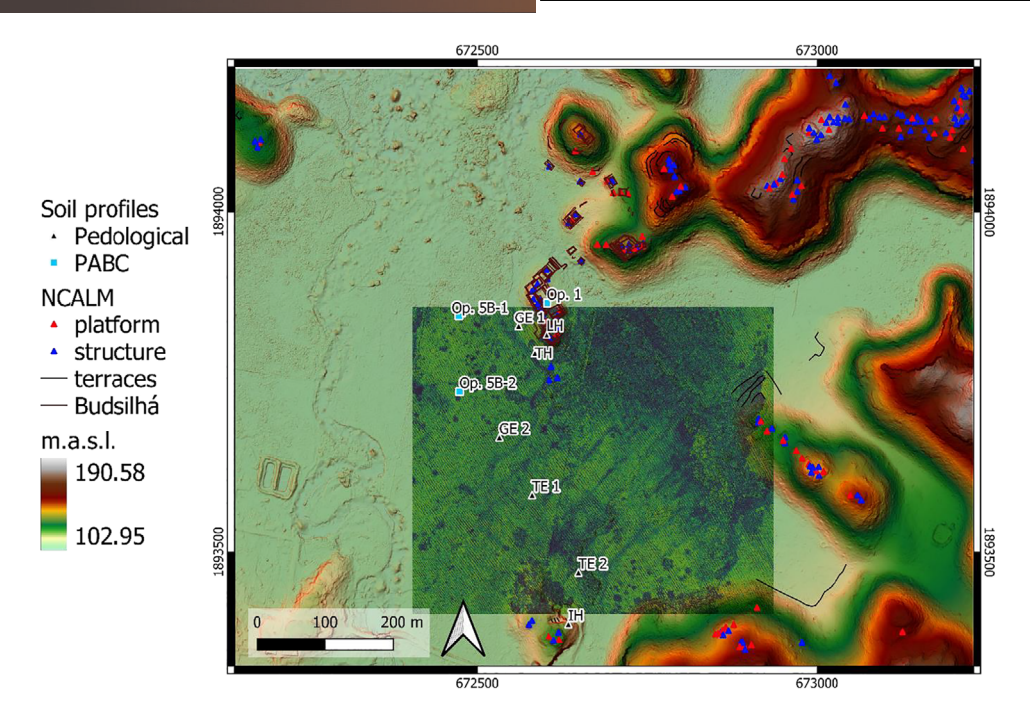


FIGURE 2 Distribution of the pedological and archaeological studied profiles in the valley of Busiljá. Pedological profiles: IH, Inceptic Haprendolls; TH, Typic Haprendolls; LH, Lithic Haprendolls; GE 1, Gypsic Endoaquepts 1; GE 2, Gypsic Endoaquepts 2; TE 1, Typic Endoaquepts 1; TE 2, Typic Endoaquepts 2. The map also shows the ancient land use. Distribution of anthropic features (platforms, structures, and terraces) in the landscape. The polyIntensity raster insert shows the canals in the swampy area near the site of Budsilhá. NCALM, National Center for Airborne Laser Mapping; PABC, Proyecto Arqueológico Busiljá-Chocoljá.

relationship between the powerful royal dynasty of Piedras Negras, and smaller royal courts in the area, including that of La Mar, located just 3.5 km southwest of Budsilhá (Houston & Inomata, 2009; Martin, 2020; Martin & Grube, 2000). Budsilhá was an important site of stone tool production during the Late Classic period (AD 600–800), and an obsidian workshop has been identified in the plaza at a habitational complex, with a density of 1723 artifacts/m³ or 320 g of obsidian/m³ from El Chayal, Guatemala (Golden et al., 2020; Roche Recinos, 2021). Given the proximity to the Busiljá River, and one of its tributaries, the principal architectural group tends to become an island with seasonal inundations of the swampy lowlands surrounding the site. This phenomenon helps to explain the settlement pattern of the area, that includes structures located on hilltops with artificial terraces on some hillslopes.

2 | MATERIALS AND METHODS

2.1 | Key soil profiles

Seven soil profiles were studied for the pedological part of the present work, along with two profiles in operations from the archaeological research (Figure 2). The profiles were selected to compare the soils in two adjacent geomorphological positions, forming a catena from the hillslopes to the lowland area. Three profiles are located on the slope of the limestone

hills, and four profiles are in a swampy depression adjacent to the hills. The archaeological profiles correspond to two operations from the 2018 field season: operation 1 located atop the central platform at Budsilhá and operation 5B in the marshy area outside the site core, north-west of probable canals identified via Google Earth Imagery (Scherer & Golden, 2018).

The soil profiles were first described in the field following the IUSS Working Group WRB (2015), and samples were taken for physicochemical, micromorphological, and mineralogical analysis at Universidad Nacional Autonoma de Mexico (UNAM). Only from archaeological excavations were samples taken for archaeobotanical investigations—phytolith and macroremains analysis—carried out at McMaster University.

2.2 | Soil chemical and physical properties

The samples recovered from the pedogenetic horizons of the key profiles were dried at 60°C for 2 days and then sifted with a 2-mm opening sieve. The analyses were completed at different laboratories at UNAM.

Particle size analysis: It is completed at the Laboratory
of Paleosoils of the Instituto de Geología, UNAM, following Flores and Alcala (2010). From the sieved sample,
10 g were used, with a pretreatment of hydrogen peroxide

 (H_2O_2) and sodium dithionite $(Na_2S_2O_4)$ to remove the cementing agents: organic matter and iron oxides, respectively. Afterward, 10 mL of sodium hexametaphosphate was added to each sample as a dispersion agent, with 25 mL of distilled water, and then the samples were agitated for 12 h. The sand fraction was separated with a sieve, and the silt and clay fractions were separated using the pipette method.

- 2. pH, electrical conductivity (EC): It is completed at the Laboratory of Biochemistry and Soil Organic Matter of the Instituto de Geología, UNAM, following Flores and Alcalá (2010). The sieved sample was prepared in a 1:2.5 ratio with distilled water and agitated for 24 h. A Thermo Scientific pH-meter was used.
- 3. Characteristics of soil solution: ionic composition by ion chromatography: It is completed in the Laboratory of Environmental Geochemistry of the Laboratorio Nacional de Geoquímica y Mineralogía, UNAM. The samples were filtered in a nitrocellulose membrane with pore size 0.45 µm. The alkalinity was determined with a 30 mL aliquot and titrated with 0.017 N HCl. An ion chromatographer Metrohm 833 Basic IC Plus with a detector of conductivity was used for the cations (Na⁺, K⁺, Ca²⁺, and Mg²⁺); a column packed with a stationary phase of silica gel model Metrosep C4 250/4.0 with a mobile phase composed of oxalic acid dihydrated with HNO3 was used; and for the anions (F⁻, Cl⁻, NO²⁻, Br⁻, NO³⁻, PO₃⁴⁻, and SO₄²⁻), polyvinyl alcohol column with quaternary ammonium groups model Metrosep A Supp 4 250/4.0 was used with a mobile phase of NaHCO₃/Na₂CO₃ with chemical suppression. This analysis was made only on groundwater samples from the soils in the lower unit (Typic Endoaquepts 1, Typic Endoaquepts 2, and Gypsic Endoaquepts 2), the samples were collected in 100-mL tubes at the time of the soil description and storage in a cooler until returning to the lab.

2.3 | Micromorphology

Thin sections were prepared from soil blocks with undisturbed structure from the key genetic horizons and impregnated at room temperature with the resin Cristal MC-40. After solidification of the resin, the blocks were cut, polished, and mounted on glass slides to obtain thin sections of 30 µm. Observations were made under a petrographic microscope Olympus model BX51 equipped with a digital camera; images were captured and processed with the help of the Image-Pro Plus 7.0 software. Micromorphological descriptions were completed following the terminology of Stoops (2020). We focused particularly on the microscopic indicators of the pedogenetic processes as well as the anthropogenic materials or microartifacts.

2.4 | Clay mineral composition by X-ray diffraction (XRD)

Granulometric clay fraction ($<2~\mu m$) was separated from bulk samples by sedimentation in distilled water according to Stoke's law, the same pretreatments for particle-size analysis were used in the samples prior to the separation. From these fractions, air-dried oriented specimens were obtained by depositing a few drops of the suspensions onto a glass slide, which was then dried at 30°C for a few hours (Moore & Reynolds, 1997). Clay samples were examined by XRD in the air-dried form, saturated with ethylene glycol (EG), and after heating (550° C). EG solvation was accomplished by exposing the slides to EG vapor at 70° C for 24 h.

Measurements were made using an EMPYREAN XRD diffractometer operating with an accelerating voltage of 45 kV and a filament current of 40 mA using $CuK\alpha$ radiation, nickel filter, and PIXcel 3D detector. All samples were measured with a step size of 0.04° (2θ) and 40 s scan step time. Qualitative identification of the most abundant clay minerals was based on the positions of basal diagnostic peaks. Clay species were estimated in semiquantitative form from oriented preparations using simple peak weighting factors. For area estimation, we used Fityk (Wojdyr, 2010), a program for data processing and nonlinear curve fitting, simple background subtraction, and easy placement of peaks and changing of peak parameters.

2.5 | Phytoliths and macroremains

In addition to pedological investigations, archaeobotanical analyses were performed on samples recovered from archaeological excavations, closely related to the key soil profiles. Sample processing at the McMaster Paleoethnobotanical Research Facility (MPERF) was conducted following the phytolith-processing protocol designed by Morell-Hart (2018). Following this protocol, phytolith samples underwent defloculation, sieving, clay removal, chemical digestion with pressurized microwaving, and heavy liquid flotation (Morell-Hart, 2018). Concentrated botanical residues were analyzed in the field laboratory, at Brown University in James Russell's laboratory in the Department of Earth, Environmental and Planetary Sciences, at Boston University in John Marston's Environmental Archaeology Laboratory, and at the MPERF.

2.6 | Study of ancient land use

Documentation of the structures related to the ancient land use of the area has been carried out through a combination of data collected by airborne light detection and ranging (LiDAR)

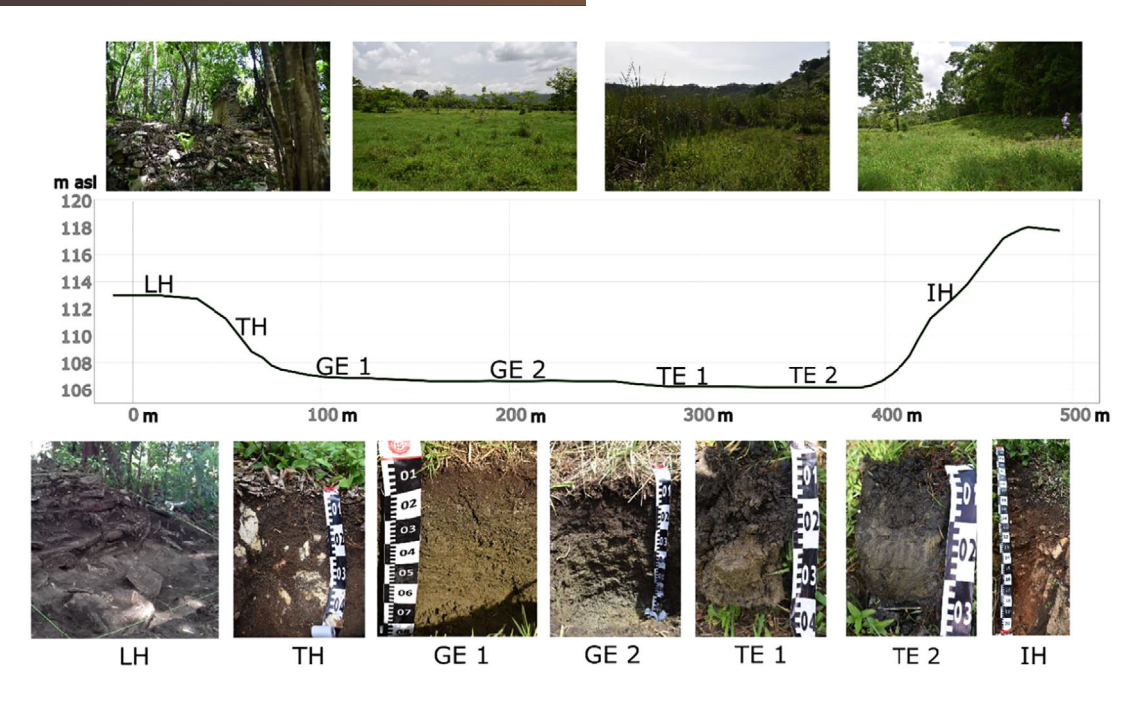


FIGURE 3 Scheme of the Busiljá soil catena and profile photos. The upland unit is comprised of the profiles Typic Haprendolls (TH), Lithic Haprendolls (LH) and Inceptic Haprendolls (IH); the lowland unit is comprised of the profiles Gypsic Endoaquepts 1 (GE 1), Gypsic Endoaquepts 2 (GE 2), Typic Endoaquepts 1 (TE 1), and Typic Endoaquepts 2 (TE 2).

and over a decade of pedestrian survey by the PABC. For the airborne LiDAR, a working group of the PABC team identified archaeological features in the National Center for Airborne Laser Mapping (NCALM) LiDAR (Golden et al., 2021), using the Relief Visualization Toolbox (Kokalj & Somrak, 2019), to create a Red Relief Image Map, a visualization for archaeological topography, and other useful visualizations. The features identified were then categorized by type of construction, like residential structures, platforms, or terraces. A PolyIntensity raster was also created from the NCALM lidar points by Whittaker Schroder, following the methodology of Beach et al. (2019) to help with the identification of features not visible in the digital elevation model and satellite imagery.

3 | RESULTS

3.1 | Morphological description of key sections

Three profiles such as: Typic Haprendolls, Lithic Haprendolls, and Inceptic Haprendolls characterize the soils developed on the limestone hills. These profiles conform to the upland unit of the studied toposequence (Figure 3, Table 1). All of them have similar profile architecture: dark loose granular A horizons of different thicknesses are underlain by the coarse calcareous regolith. These A horizons fit into definition of Mollic epipedon. Thus, all these profiles were

attributed to the Rendoll suborder of soil taxonomy (Soil Survey Staff, 2022).

The Inceptic Haprendolls Profile is located close to the top of a minor hill near the Budsilhá site and exposed in a small quarry for limestone extraction. The A horizon continuously covers the hill surface; however, the middle and lower horizons are developed inside a thin and deep (down to 2 m) karstic pocket filled with pedosediment; that is why this profile is the deepest in the Rendoll group. It consists of a A1-A2-B-BC sequence of horizons. The loose, granular, dark gray A horizon extends down to 80 cm, followed by a reddishbrown B horizon with presence of anthropogenic materials (ceramic sherds, bones, shell, and charcoal). The rest of the profile is a BC horizon with abundant fragments of limestone.

The Typic Haprendolls profile is located at the lower slope of the limestone hill, upon which the ancient Maya settlement of Budsilhá was constructed. It is a thin soil of only 25-cm deep with a sequence of horizons typical of an incipient soil: A-AB-BC. Differences between the horizons consist mostly of an abundance of stones which increases with depth and reaches approximately 80% in the BC horizon. The fine soil material is dark colored with granular structure most developed in the A horizon. It contains archaeological materials: several ceramic sherds and charcoal.

The Lithic Haprendolls profile is located on top of limestone hill above an archaeological structure in the site of Budsilhá; it represents the soil formation after the abandonment of the site at the end of the Classic Period (900 AD). It is very shallow and consists of only one dark-colored granular

TABLE 1 Soil properties of the studied profiles.

		a	Q.		Consistence		
Horizon		Color (dry)	Structure		(dry)	HCl reaction	Observations
_	_	N 672634.46°E 1					
A1	0–30	7.5YR 2.5/2	GR	Clay loam	1	+	Presence of roots
A2	30–80	7.5YR 2.5/2	GR	Silty clay	1	++	Presence of roots
В	80–130	7.5YR 5/6	SB	Clay	2	+++	Anthropogenic materials (ceramics, bones, charcoal)
_	130–140	ND	ND	ND	ND	ND	Limestone rock slabs Anthropogenic materials
BC	140-200	7.5YR 5/8	MA	Silty clay	0	ND	Calcareous parent material
Typic Hap	rendolls 15N	672584.44°E 189	3792.33°N				
A	0–12	7.5YR 2.5/3	GR	Clay	1	NR	Presence of roots
AB	12–25	7.5YR 3/4	SB	Silty clay	2	+	High pedregosity (40%) Anthropogenic materials
BC	>25	7.5YR 3/3	SB	-	3	++	High pedregosity (60%)
Lithic Ha	prendolls 15N	672602.17°E 189	3792.48°N				
A	0–10		GR	Silt loam	1	NR	
Typic End	loaquepts 1 15	N 672560.46°E 1	893832.09°N				
Ag	0–15	10YR 3/1	GR	Clay	2	NR	Gleyic properties
Cg	15-30	10YR 5/4	SB	Clay	3	NR	Gleyic properties
Gypsic Er	doaquepts 1 1	5N 672580.26°E	1893584.48°	N			
AB	0–15	10YR 3/3	SB	Clay	2	NR	
Ву	15–25	10YR 4/4	SB	Clay	4	NR	Coarse sand size gypsum crystals
Cgy1	25–52	10YR 4/3	AB	Clay	3	NR	Gleyic properties and gypsum crystals
Cgy2	52–80	10YR 4/3	AB	Clay	3	+	Increase the presence of large gypsum crystals
Gypsic Er	doaquetps 2 1	5N 672532.26°E	1893668.93°	N			
A	0–15	10YR 2/1	GR	Clay	2	NR	Presence of roots
Cgiy	15–40	10YR 3/2	AB	Silt clay	3	NR	Slickensides, and neoformed gypsum
Cgy	40–70	10YR 3/2	SB	Clay	3	+++	Presence of neoformed gypsum
Typic End	loaquepts 2 15	N 672649.2°E 18	93470.08°N				
Ag1	0–15	10YR 2/1	GR	Clay	2	NR	Abundance of fresh roots
Ag2	5–15	10YR 2/1	GR	Clay	2	NR	Gleyic properties
Cg	15–25	10YR 4/2	SB	Clay	2	++	Gleyic properties, limestone and snail fragments
2Ag	25–35	10YR 3/2	SB	Clay	2	NR	Presence of decomposed roots

Note : Consistence = 0: Loose, 1: Soft, 2: Slightly hard, 3: Hard, 4: Very hard; HCl reaction = +: low, ++: medium, +++: strong.

Abbreviations: AB, angular blocky; GR, granular structure; MA, massive; ND, not determined; NR, no reaction; SB, subangular blocky structure. The codes of color are presented following the Munsell Color Chart.

A horizon directly underlain by a large limestone slab—part of ancient Maya construction.

The second group consists of four profiles located in the flat depression between the limestone hills, which represent the lowland domain of the Busiljá catena. These are deep loamy-clayey soils; major part of their profile is permanently saturated with groundwater, and during the period of intensive rains, they are flooded. They do not have high accumulation of organic matter in the form of peat, sapric materials, or dark humus; however, all their horizons show

strong redoximorphic features; we concluded that these profiles belong to Endoaquepts Great Group. The profiles could be grouped into two units, related to their position within the depression.

Soils of the lowest part of the depression are represented by the Typic Endoaquepts 1 and 2 profiles. Groundwater was so near to the surface that description and sampling were done in the soil blocks cut and uplifted with the spade—this limited the depth of the studied section to 30 cm. In Typic Endoaquepts 1, only two horizons were identified: Ag-Cg, both with strong gleyic properties such as pale greenish color and ferruginous mottles. Typic Endoaquepts 2 profile, located close to the foot of the limestone hill where Typic Endoaquepts 1 was described, has an additional pale brown 2Agb horizon below Cg.

Slightly elevated part of the depression, adjacent to the hill where Budsilhá site is located, is represented by the profiles Gypsic Endoaquepts 1 and 2. The groundwater level here is lower that allowed us to study sections down to 80 cm. Grayish-brown humus Ag horizon is underlain, from 15 cm downward, with a set of ABgy-Cgy1-Cgy2 horizons of reduced greenish color with gleyic and—unexpectedly—gypsic properties. The presence of neoformed gypsum crystals is evident in the field; they are observed as white powdery mottles directly below the A horizon, while deeper large clearly visible gypsum crystals of several millimeters in length were also found. We propose to define these complex profiles as Gypsic Endoaquepts, although such a subgroup is not specified in the Keys to Soil Taxonomy (1998).

3.2 | Soil physical and chemical properties

According to the results of the particle size analysis, the studied soils have relatively high clay content. Already in the upland profile, Inceptic Haprendolls clay content reaches 40% in the A horizons, increasing to more than 50% in the B horizon. In the hydromorphic soils of the depression area, clay content is even higher, reaching 60%–80% in the Typic Endoaquepts 2, Gypsic Endoaquepts 1 and 2 sections. Within the coarser material, silt fractions are more abundant. Only in the upper A horizon of Inceptic Haprendolls is a strong increase of sand (more than 30%) observed (Figure 4).

pH values in all profiles vary in the range from 6 to 8; similar pH ranges were observed both in the upland profiles and in the depression. In the profiles Inceptic Haprendolls and Gypsic Endoaquepts 2, we observed decrease in the pH values in the upper horizons, an expected tendency explained by the enrichment of topsoil with carbon dioxide and organic acids due to decomposition of the plant residues. The opposite trend was documented in the profile Typic Haprendolls—probably generated by the downslope redeposition of carbonate materials. The behavior of the EC is much more variable. The upland profiles have moderate values: in the range 200–500 μS/cm in the profile Inceptic Haprendolls and 600-800 in Typic Haprendolls. Much higher conductivity is encountered in the hydromorphic profiles within the depression: 1000-2000 µS/cm in Typic Endoaquepts 2 and even more than 2400 μS/cm in the profiles Gypsic Endoaquepts 1 and 2 (Figure 4).

Water from the swamp in the Typic Endoaquepts 1 had a pH of 6.4 and an EC of $1760\mu S$ at $33^{\circ}C$, and in the Typic Endoaquepts 2, a pH of 7.49 and an EC of $600~\mu S$ at $32^{\circ}C$ were observed.

Results from the analysis of the ionic composition of soil solutions obtained directly from the hydromorphic profiles show that in the profiles without morphological evidence of gypsum neoformation—Typic Endoaquepts 1 and 2—the dominant anion was hydrogen carbonate ion (HCO³⁻), whereas among the cations Ca^{2+} and Mg^{2+} were present in similar quantities. On the contrary, in the gypsiferous profile Gypsic Endoaquepts 2, the anion pool was dominated by sulfate (SO_4^{2-}), and among cations Ca^{2+} prevails (Figure 5).

3.3 | Micromorphological observations

In the profile Inceptic Haprendolls, the A horizon is characterized by very high porosity, strong development of structure conformed by granules and small rounded blocks, pigmentation of the groundmass with dark humus and frequent plant residues showing different degrees of decomposition (Figure 6a). The B and BC horizons of this profile show a quite different arrangement: they are compact, and pores are few, being presented mostly by tortuous fissures which delimit larger subangular blocks (Figure 6b). The groundmass has reddish-brown color due to ferruginous pigment. This groundmass contains abundant carbonates—both coarse particles of irregular shape and micrite incorporated into the fine material. However, we observed some aggregates free of carbonate particles; they consist only of clay and iron oxides and have much stronger red pigmentation than the host material (Figure 6c). Clay component of these aggregates does not show any birefringence. Various human-introduced components were observed throughout the profile, especially in the B horizon: fragmented mollusk shells (Figure 6d), bone (Figure 6e), and charcoal particles (Figure 6b).

The groundmass in the A and AB horizons of the Typic Haprendolls profile is also enriched with dark humus and contains carbonates—coarse particles and micrite. Human-introduced components are few, although some small charcoal particles were encountered (Figure 6f). As in the case of the Inceptic Haprendolls profile, here we also observed aggregates of red clayey-ferruginous material free of carbonates, also with undifferentiated b-fabric (Figure 6g,h).

Micromorphological observations in the Gypsic Endoaquepts 1 profile revealed a quite specific set of pedogenetic features. The matrix of its Ag horizon is moderately pigmented with humus; however, it is rather compact and has blocky structure. Clusters of zoogenic aggregates—excrements of mesofauna—are few and encountered only within the fragments of plant tissues. In the lower C horizons, the material becomes even more compact, and the ground-mass is comprised mostly of clayey fine material. Contrary to the upland profiles, the clay component here shows rather strong interference colors, producing speckled and striated b-fabric. Few rounded iron-manganese nodules are immersed in

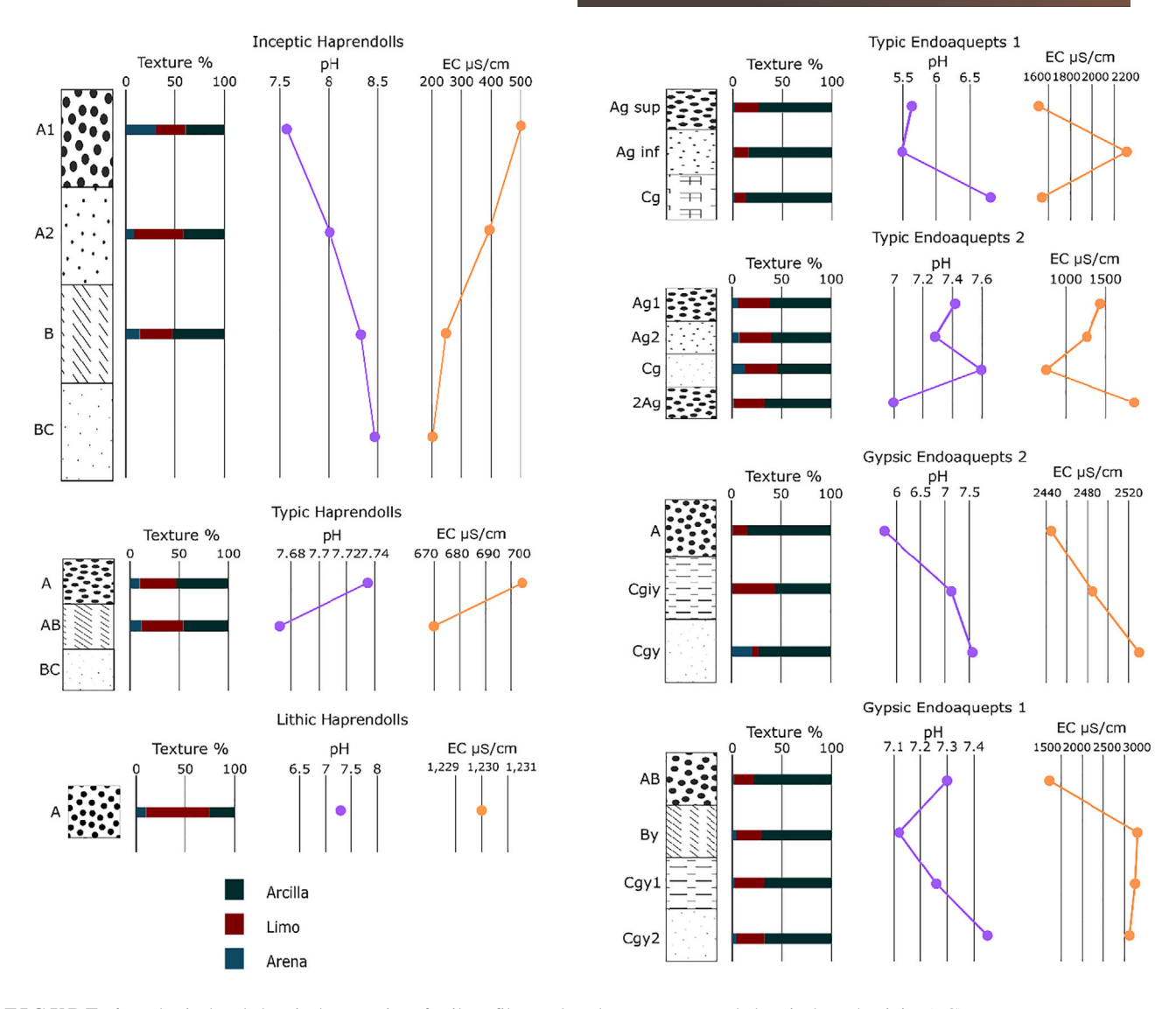


FIGURE 4 Physical and chemical properties of soil profiles analyzed: texture, pH, and electrical conductivity (EC).

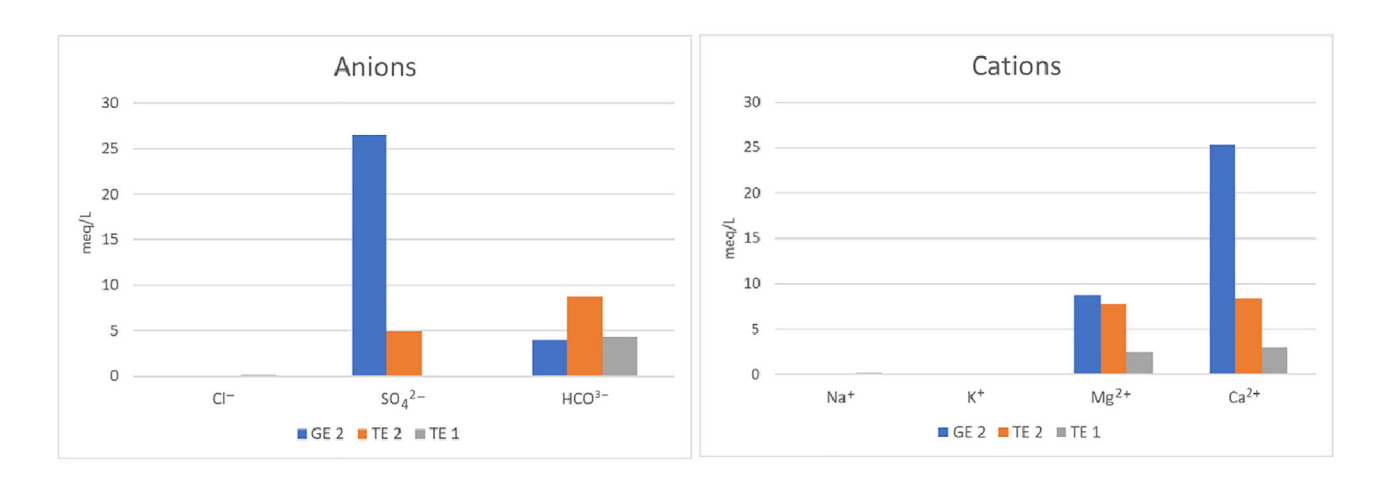


FIGURE 5 Ionic composition of soil solutions from the hydromorphic profiles: TE 1, Typic Endoaquepts 1; TE 2, Typic Endoaquepts 2; and GE 2, Gypsic Endoaquepts 2.

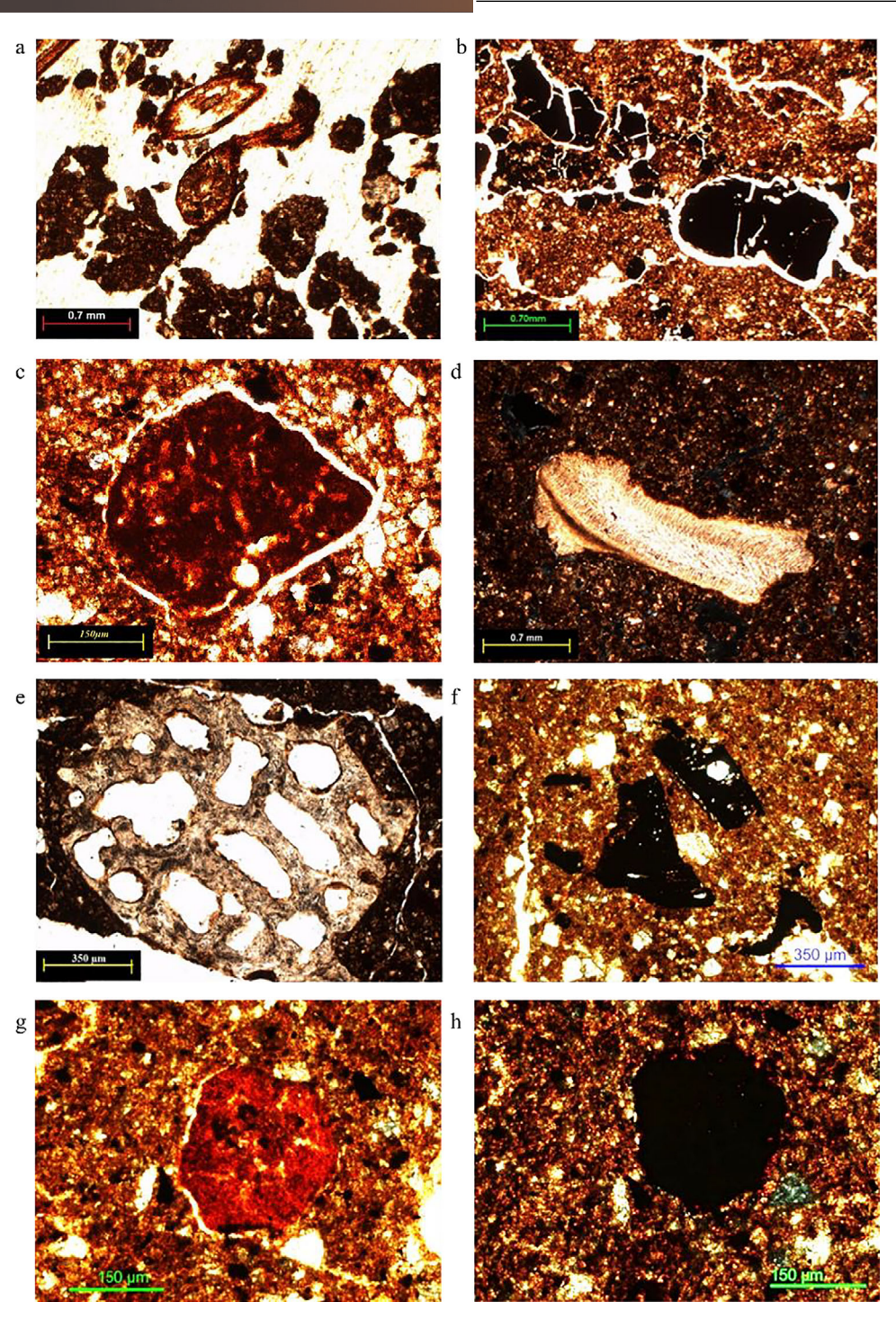


FIGURE 6 Micromorphology of the upland soils. (a)–(e) Inceptic Haprendolls profile: (a) Coprogenic structure, high porosity, fragments of partly decomposed plant tissues; A horizon, PPL. (b) Compact arrangement, few fissures, black charcoal particles; B horizon, PPL. (c) Aggregate enriched in clay and ferruginous pigment, free of carbonates; BC horizon, PPL. (d) Fragment of mollusk shell; B horizon, N+. (e) Porous bone fragment; B horizon, PPL. (f)–(h) Typic Haprendolls profile: (f) Charcoal particles incorporated into compact groundmass; AB horizon, PPL. (g) Aggregate enriched in clay and ferruginous pigment, AB horizon, PPL. (h) Same as (g), N+, note abundant micritic and sand-size carbonate particles with strong interference colors in the groundmass, whereas in the clayey aggregate such particles are absent. PPL, plain polarized light; N+, crossed polarizers.

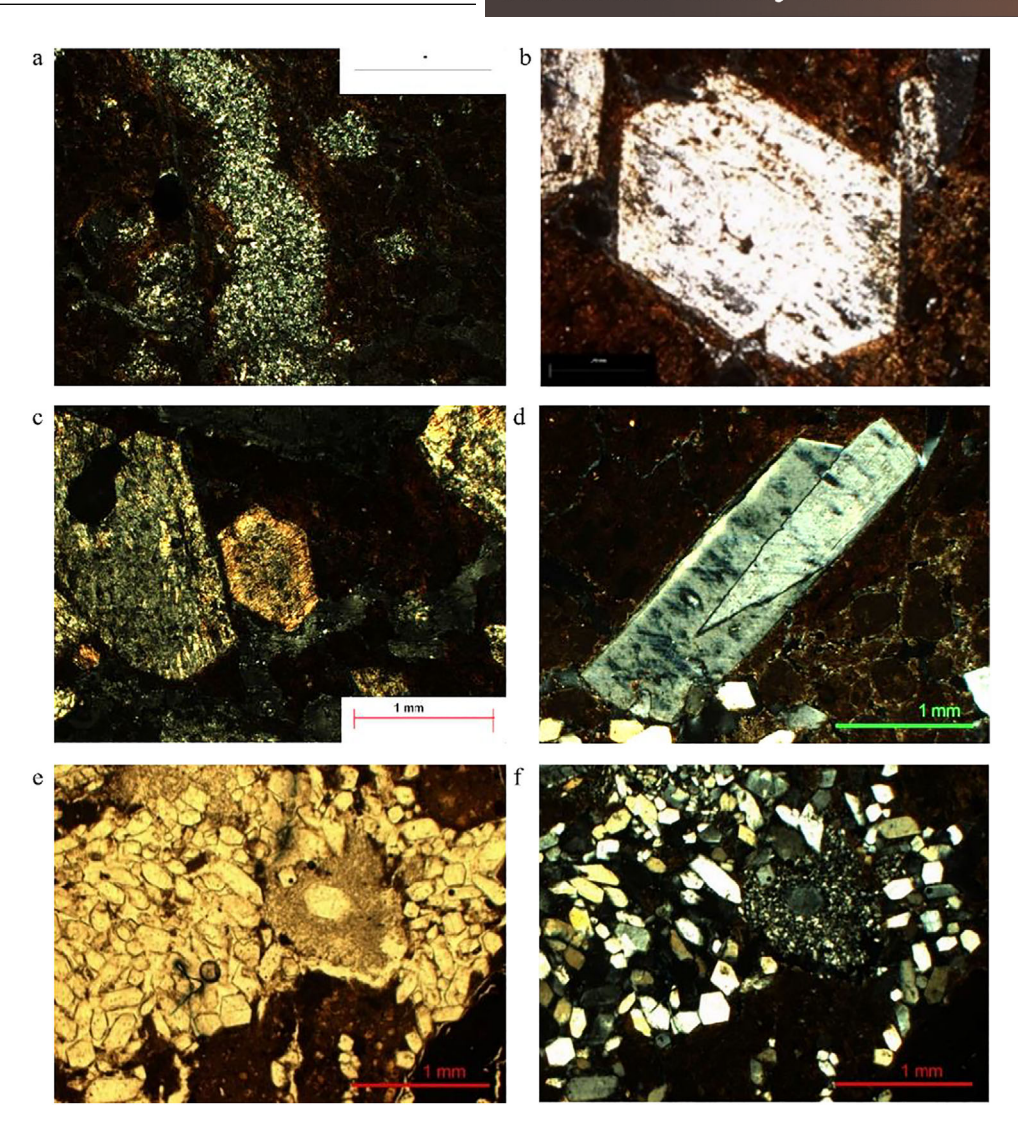


FIGURE 7 Micromorphology of the lowland gypsiferous soil, all photos under crossed polarizers. (a)–(c) Gypsic Endoaquepts 1 profile: (a) Compact microcrystalline gypsum infilling in a large pore, A horizon. (b) Large isometric tabular crystal of gypsum, C horizon. (c) Zonal tabular gypsum crystal, C horizon. (d)–(f) Gypsic Endoaquepts 2 profile: (d) Large elongated twinned crystal of gypsum, Cr horizon. (e) Heterogeneous gypsum infilling: clusters of microcrystalline particles are surrounded by larger sand-size grains, Ag horizon. (f) same as (e) under crossed polarizers.

the clayey groundmass. The most peculiar observation in this profile is the abundance of neoformed gypsum pedofeatures. In the A horizon, these features are presented by compact microcrystalline infillings in the pores (Figure 7a). Below, in the C horizons, large isometric tabular crystals appear (Figure 7b), and some of them are zonal (Figure 7c). No signs of dissolution or degradation of gypsum, like etching pits, substitution by carbonates, or penetration of clayey material, were observed. The Gypsic Endoaquepts 2 profile has rather similar micromorphological characteristics. However, it shows some additional features of neoformed gypsum. In the Cr horizon, we encountered elongated gypsum crystals (Figure 7d). We observed variability of crystal sizes within a single pedofeature: within the infillings in the Ag horizon, clusters of microcrystalline particles are surrounded by larger sand-size grains (Figure 7e,f).

In the lowermost Typic Endoaquepts 2 profile, some areas with zoogenic granular structure are observed (Figure 8a) only in the uppermost part of the A horizon, while other parts of the profile are compact and blocky. Groundmass is clayey, pigmented with humus. Numerous plant tissue fragments show different stages of decomposition but no signs of mesofauna activity (Figure 8b). Human-introduced components (microartifacts) were practically invisible with the exception of very few quite small charcoal particles in the Ag horizons (Figure 8c). Below, in the Cr horizon, clayey fine material shows rather strong interference colors, groundmass incorporates rounded Fe-Mn nodules, better developed in the profile Typic Endoaquepts 1 (Figure 8d). These features are quite similar to the lower parts of the Gypsic Endoaquepts profiles. However, in the Typic Endoaquepts profiles, no neoformed gypsum was encountered. Also, no carbonates (coarse

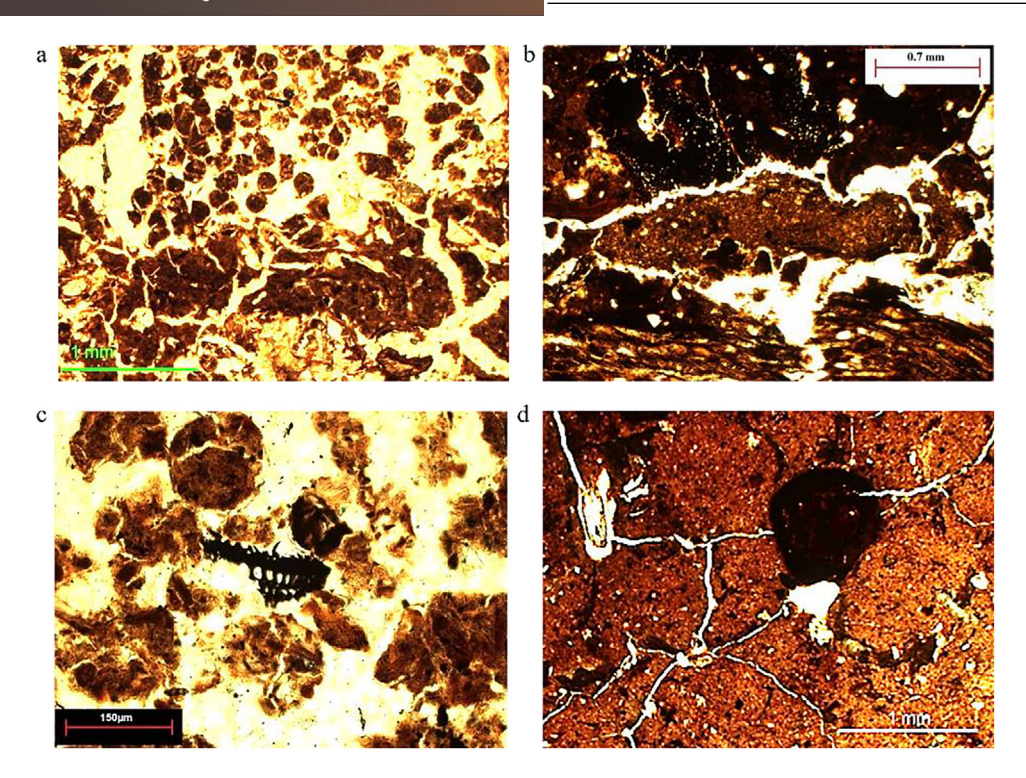


FIGURE 8 Micromorphology of the lowland swampy soils without gypsum, all photos under plain polarized light. (a)–(c) Profile Inceptic Haprendolls, Ag horizon: (a) Area with zoogenic granular structure in the upper part of the viewfield, neighboring blocky structure in the lower part, Ag horizon; (b) large fragments of plant tissues, strongly decomposed; and (c) small charcoal fragment. (d) Typic Endoaquepts 1 profile, Cr horizon: ferruginous nodule within the clayey groundmass.

or micritic) were observed in groundmass of any lowland soils. Human-introduced components (microartifacts) were practically invisible with the exception of very few quite small charcoal particles in the Ag horizons (Figure 8d).

3.4 | Clay mineral assemblages

Clay mineral assemblages were studied in the samples from selected horizons of the profiles (B horizon of the Inceptic Haprendolls profile, AB horizon in the Typic Haprendolls profile, Cgy1 horizon of the Gypsic Endoaquepts 1 profile, Cg horizon in the Typic Endoaquepts 1 profile, and C in the Inceptic Haprendolls profile), to use as an indicator of the weathering status and a tracer of the provenance of soil mineral mass. Despite contrasting differences of the morphological and physicochemical properties, all soils of the studied chronosequence showed a similar composition of the clay mineral assemblages. Below, we list the main identified clay components and briefly describe their diagnostics by XRD, according to the position of diagnostic peaks and their reaction to the applied pre-treatments.

In all studied samples, we observed major abundance of a group of 2:1 clay minerals that produced prominent 1.4 nm basal spacing in the air-dry sample. Within this group, the following individual components were discriminated: (1) Ver-

miculite: 1.4 maximum remains unchanged after glycolation but shifts to 1.0 nm after heating. (2) hydroxy-interlayered vermiculite (HIV) is differentiated from normal vermiculite by an incomplete shift of the 1.4 nm maximum after heating: it is expressed in asymmetry of the 1.0 nm peak that had a clear "shoulder" toward smaller angles. This asymmetry is interpreted as evidence of the incomplete collapse of the vermiculite structure after heating caused by the presence of a fragmentary additional octahedral layer, characteristic for HIV (Barnhisel & Bertsch, 1989), also called "soil chlorite." (3) Smectite is characterized by a shift of 1.4 nm maximum to smaller angles after glycolation, producing a spacing of 1.5–1.6 nm. Smectitic component is also recorded by the behavior of the 0.7 nm maximum which is displaced after glycolation to approximately 0.76 nm.

The second most abundant component is kaolinite that produces well-defined 0.7 nm basal spacing in the air-dry sample that stays unchanged after glycolation but disappears in the samples heated to 550°C. Finally, illite is detected by the 1.0 nm basal peak, that is not modified by the pre-treatments; this component is present in minor amounts since it only appears as a small shoulder of the 1.4 nm peak.

The proportions of the components within the clay mineral assemblages differed significantly in the upland Rendolls and lowland Endoaquepts. In all the samples of the upland unit, we found only two defined components, the strongest

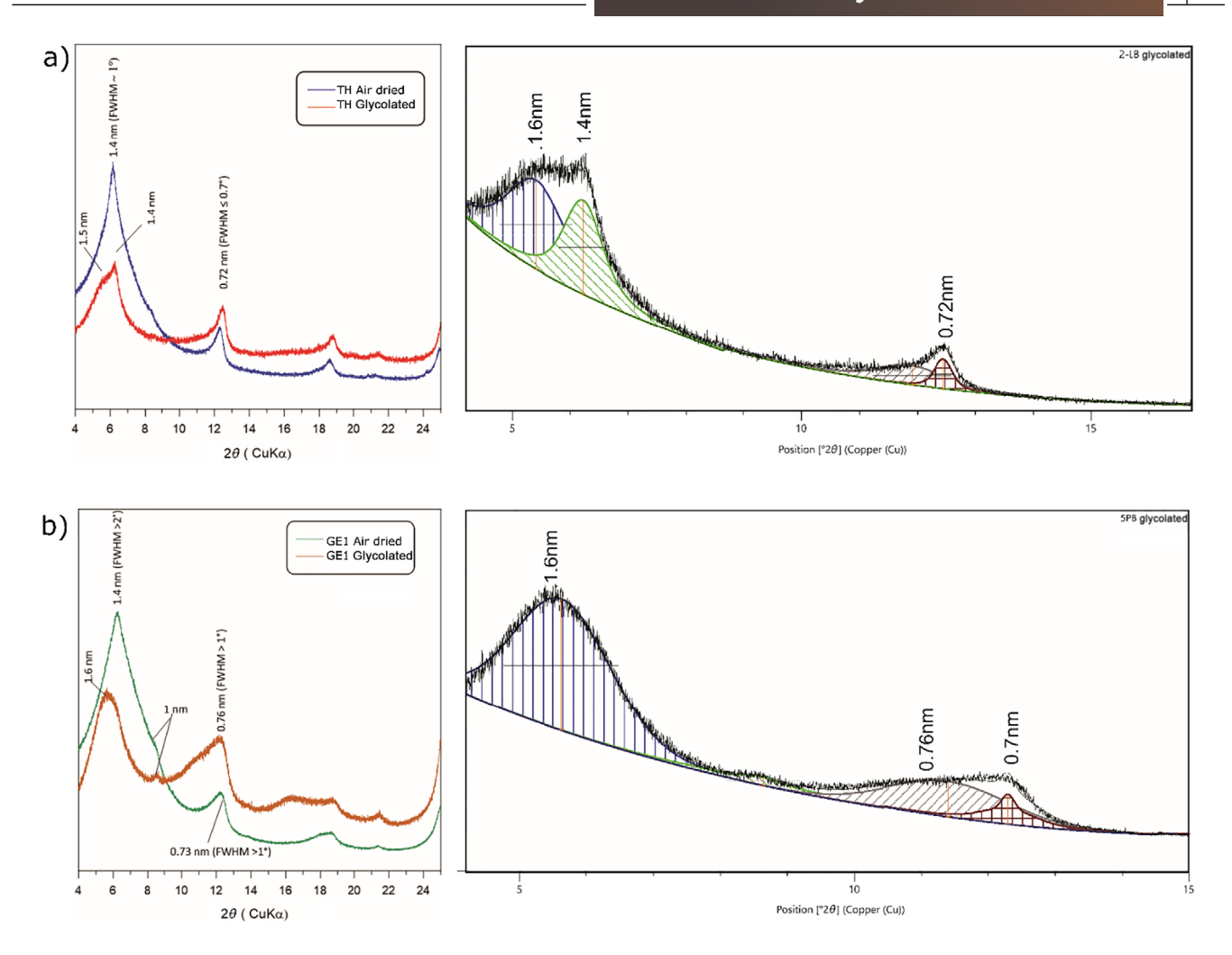


FIGURE 9 Difractograms: (a) Upland Unit: TH, Typic Haprendolls and (b) Lowland Unit: GE 1, Gypsic Endoaquepts 1. FWHM, full width at half maximum.

one of 1.4 nm and the other of 0.7 nm of basal spacing. The 1.4 nm peak in the air-dried sample has full width at half maximum (FWHM) values close to 1 (intermediate crystallinity). The 1.4 nm component splits in two when the sample is glycolated; one remains at 1.4 nm, and the other partially expands to 1.5 nm. The non-expansive component predominated and shifted to approximately 1.0 nm after heating at 550°C. The expansive component is not very relevant. In all diffractograms of the heated specimens, we observed clear asymmetry of the 1.0 nm peak of the collapsed vermiculite: it had a clear "shoulder" toward smaller angles. We interpret this observation as evidence of the incomplete collapse of the vermiculite structure after heating caused by the presence of a fragmentary additional octahedral layer. This component could be interpreted as HIV (Barnhisel & Bertsch, 1989), also called "soil chlorite." The 0.7 nm component is not modified in glycolation, but disappears when heated, thus, it is interpreted as kaolinite that has high crystallinity (FWHM \leq 0.7). The 1.0 nm illitic component is only observed in one sample in a very small proportion, <5% (Figure 9a, Table 1).

In all the samples of the lowland unit, we found three components, one of 1.4 nm, a second of 1 nm (minority), and another of 0.7 nm of basal spacing. The 1.4 nm peak in the untreated sample has higher FWHM values (lower crystallinity) than the upper samples. The 1.4 nm component does not split upon glycolation and expands to about 1.6 nm. The expansion is clearer than for the samples of the upper unit; for this reason, it is interpreted that the smectitic component is the predominant one. Such modification by expansion can also be observed in the 0.7 nm peak. The HIV or smectite component is minor, but still is observed in the heated samples, as indicated by incomplete collapse of the vermiculite structure after heating. The component of 0.7 nm is modified in the glycolation; it has low crystallinity (FWHM > 1) and is interpreted mainly as smectitic type, but also with the contribution of kaolinite (in some samples, the presence of the two differentiated peaks can be observed). The peak located at 1.0 nm corresponds to illite of low crystallinity and is found only in the samples of this lower unit and is always a minority phase since it only

TABLE 2 Semiquantitative values obtained using Fityk (Wojdyr, 2010) software.

	Sample		Typic Haprendolls	Inceptic Haprendolls
Upland Unit	Smectitic component		XX	XX
	Vermiculite and hydroxy	-interlayered vermiculite (HIV)	XXXX	XXXX
	illite		(X)	(X)
	Kaolinite		X	X
	Sample	Typic Endoaquepts 1	Gypsic Endoaquepts 1	Typic Endoaquepts 2
Lowland Unit	Smectitic component	XXX	XXXX	XXXX
	Vermiculite and HIV	XX	X	XX
	Illite	X	X	X
	Kaolinite	X	X	X

Note: (X) = <5%; X = 5%-15%; XX = 15%-30%; XXX = 30%-50%; XXXX = >50%.

appears as a small shoulder of the 1.4 nm peak (Figure 9b, Table 2).

3.5 | Phytoliths and macroremains

The excavations at Op.1, in the Central platform at Budsilhá, revealed a number of charred remains from wild and/or managed plants. The BU-01-B-05-04 excavation unit yielded a domesticated tomatillo (cf. *Physalis ixocarpa* Brot. ex Hornem) seed at an upper anthropogenic level, and a cf. chile pepper (*Capsicum annuum* L.) seed, maize (*Zea mays* L.) cupule, and cactus fruit (*Melocactus* sp.) seed in a lower, earlier level (BU-01-B-05-06; Figure 10). An even earlier anthropogenic deposit in the BU-01-B-05-07 unit yielded a nance (*Byrsonima crassifolia* L.) fruit seed. All these charred botanical remains come from primary or secondary deposits identified as construction fills, and do not represent plants grown in situ atop the constructed platform.

The excavations at Op 5B, in the swampy area, lots 2 and 3 of unit BU-05-B-01, yielded no preserved or identifiable remains from domesticated plants, though they did reveal several charred remains and phytoliths from wild and/or managed plants of the Onagraceae, Asteraceae, Solanaceae, Verbenaceae, Vitaceae, Polygonaceae, Poaceae, and Chenopodiaceae families. Decorated spherical phytoliths likely from the palm family were also recovered in this unit. Unit BU-05-B-02 yielded no botanical remains that could be identified even to family, and no artifacts.

3.6 | Ancient land use

Analysis of LiDAR and pedestrian archaeological surveys in the study region have helped to clarify ancient settlement patterns. Archaeological features, including residential structures, platforms, terraces, and canals, are distributed through the geoforms (Figure 2).

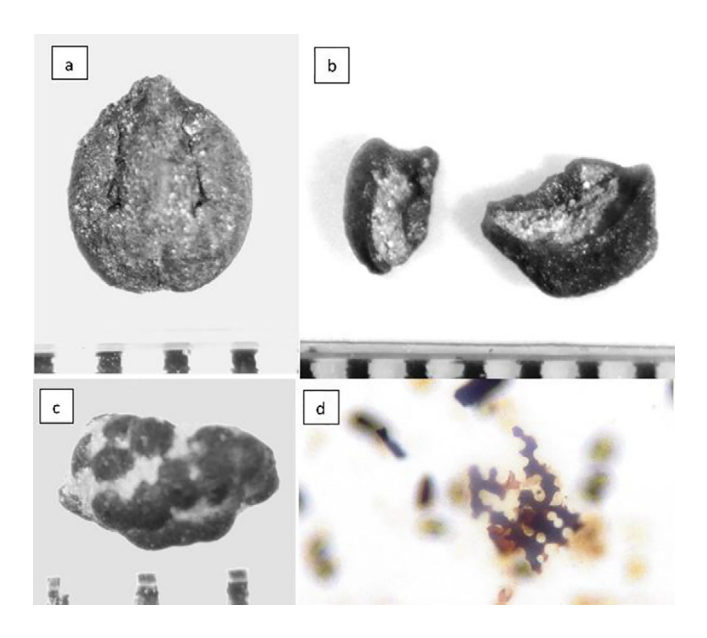


FIGURE 10 Examples of phytoliths and macroremains. (a) Seed of Caribbean grape (*Vitis tiliifolia* Humb & Bonpl. ex Schult.) (BU-1-B-05-02-LF), (b) cupules of *Zea mays* (BU-1-B-05-04-HF), (c) fragment of a seed of *Melocactus* sp. (BU-1-B-05-06-LF), and (d) perforated opaque phytolith corresponding with the sunflower family (Asteraceae).

Constructed platforms and structures are located on the upper parts of the terrain, atop mountains or hills, as is the case for some architecture at Budsilhá and the site on top of the hill in Rancho Maria, the hill where the Inceptic Haprendolls profile is at.

Constructed terraces are present in the upper and lower parts of the terrain, although they are more visible in the upper zones. They are present in slopes close to the valley bottom or near the top of the mountains, close to the platforms and structures.

In higher zones, where slope could have been an issue for settlement construction, terraces were probably more frequently used for habitation purposes and potentially home gardens, while terraces in lower zones of the terrain could have been more frequently used for agricultural purposes, as far as their soils are deeper and more fertile due to colluvial pedosediment accumulation. The more frequent use of lower zones for agricultural production is additionally supported by the presence of rectilinear canals, identified through the PolyIntensity raster (Figure 2).

4 | DISCUSSION

4.1 Upland soils: Human-induced erosion and development of shallow upland Rendolls

Soil profiles developed on the limestone hills (which host the ruins of ancient buildings and rich cultural layers with artifacts) are composed predominantly of thin dark humus horizons underlain by continuous limestone, coarse limestone colluvium or debris from collapsed constructions—also calcareous. Indeed, profiles Typic Haprendolls and Lithic Haprendolls are of this kind, whereas in the Inceptic Haprendolls profile under humus horizons, we observed a deeper solum (Bw and BC horizons)—but only locally, in a thin karst pocket. The morphology of these profiles might suggest that they be interpreted as quite primitive soils, a product of incipient pedogenesis. However, from our viewpoint, this is a deceiving impression: the properties of soil mass disagree and point to an alternative explanation. The granulometric analysis points to relatively high content of clay fraction. Micromorphological observations show that although some carbonates (mostly primary) are present in the groundmass, its larger part consists of silicate clay. Further mineralogical investigation by XRD revealed the composition of clay: it is dominated by vermiculite (including HIV) and kaolinite (Table 1). These components indicate the intermediate to high weathering status of these soils that require an advanced stage of pedogenesis under leaching and acidification conditions (Dixon, 1989; Douglas et al., 1989). We strongly doubt that abundant neoformation of these clay components could take place within the soil environment of a thin calcareous alkaline soil because in such medium, acidic products of organic matter decomposition—that are the main agents of weathering and clay mineral formation—should be quickly neutralized by calcium carbonate. Thus, we suppose that they are inherited from a different soil system, now absent in the studied geoforms.

Micromorphology provides hints to infer characteristics of this pre-existing soil on the limestone hills. In the profile Inceptic Haprendolls and profile Typic Haprendolls, we observed fragments of red clayey soil material free of calcite, immersed in the humic or in the carbonate host groundmass. We speculate that these fragments are inherited from a thick ferruginous clay-rich soil originally developed on the

limestone hills of Busiljá. Such soils are common for pedogenesis on karstified carbonate rocks, especially in subtropical and tropical regions, and have been referred to as Terra Rossa (e.g., Mediterranean basin, Southern China, Caribbean, among others), and their genesis remains a subject of discussion (e.g., Cabadas-Baez et al., 2010b; Merino & Banerjee, 2008). These soils were found in the mountainous landscapes of Chiapas (Solís-Castillo et al., 2014) and were observed in some exposures close to the study area in similar geomorphic positions but without evidence of anthropogenic activity (see Arriva Cueva profile in Sedov et al., 2023). We suppose that Terra Rossa soils once covered the limestone hills of Busiljá but have been destroyed by erosion. The residues of these soils are presented by the still recognizable red clayey microfragments incorporated into the slope colluvial soils (Typic Haprendoll profile) or into the fills of karstic hollows (as in Inceptic Haprendoll), and also by the fine kaolinitic-vermiculitic material, mixed with humus and lithogenic carbonates in the groundmass of the upper dark horizons of the Rendoll soils. The latter are strongly affected by soil fauna activity that is evidenced by their well-developed granular structure of coprogenic origin. This activity results in pedoturbation and translocation of fine soil material toward the surface and could be responsible for development of dark soils over archaeological monuments. This is a wellknown phenomenon described already by Darwin (1881) who attributed soil development on ancient Roman ruins to the continuous earthworm activity.

Soil erosion in the upland areas, to a large extent, could have been provoked by ancient Maya land use. Construction and settlement activities are documented by the PABC archaeological excavations and LiDAR data, mostly on the calcareous hills. Such activities would be accompanied by the destruction of natural vegetation and soil disturbance, precursors to erosion processes. The presence of macro- and microscopic artifacts associated with redeposited red soil fragments in the Rendolls supports the supposition of mostly human-induced colluviation process. Large-scale human-induced erosion of soils in the upland areas and deposition of pedosediments in the lowlands, which started in the preclassic and culminated during the Classic period, have been documented in various Maya regions (Beach et al., 2006, 2018). In the Yucatan peninsula, erosion of Terra Rossa soils and their substitution by dark shallow Rendolls was accompanied by deposition of large amounts of red pedosediments in the underground karstic hollows: sinkholes and cave floors (Cabadas-Báez et al., 2010a; Sedov et al., 2023). We further speculate that in the study area, erosion provoked by humans took place rather early. Excavations at Budsilhá and other neighboring sites have not revealed red soils below the constructions and cultural layers of the Classic period. This means that already before the development of these settlements, deep red soils were largely eroded due to earlier Preclassic landuse, thus the timing of earliest

land degradation processes in the region is set before 1.7–2 kyr BP, in agreement with paleopedological results from the other Maya regions of Southern Mexico (Sedov et al., 2023).

In terms of environmental and agronomic quality, the major problem with the upland Rendolls is their shallow and uneven thickness. On the other hand, high humus content and well-developed structure are beneficial properties for agriculture. At present, these soils are not targeted for cultivation, however, they support abundant natural selva vegetation that has developed on the abandoned Classic Maya settlements. These soils could also have been used by ancient inhabitants for planting homegardens within the settlement areas, thought to be an important part of Maya agricultural land-scapes (Morell-Hart et al., 2023). To cope with the small and variable thickness of Rendolls, high-precision "container gardening" technology could have been applied (Fedick et al., 2008; Flores-Delgadillo et al., 2011).

4.2 | Lowland soils: Possible impact of redeposition, the origin of gypsum, potential for ancient agriculture

The hypothesis of strong erosion as a key factor of soil evolution on the calcareous hills should have some implications also for the lowland areas, which should receive at least part of the eroded material, leaving identifiable footprints. At first glance, we do not find these eroded materials in the studied profiles, apart from small charcoal fragments that could be in situ. No features that could be attributed to the pedosedimentary material were observed at the macro- or microscale. However, we speculate that the clay minerals could provide a hint for detecting redeposition. Clay mineral assemblages show a striking similarity in the upland and lowland profiles despite their contrasting morphological differences (Table 1). In both cases, the clay mineral assemblage is constituted by two major components: 1.4 nm—vermiculite and smectite, with different grades of chloritization and 0.7 nm— kaolinite. This similarity is uncommon by far in tropical soil toposequences. Usually, the mineralogy of elevated positions and depressions differs significantly because of contrasting weathering intensities, controlled by drainage (Duchaufour, 1982). For example, in classic "black and red" toposequences, the clay of well-drained slope soils consists mostly of kaolinite, whereas smectites dominate in depressions (Kantor & Schwertmann, 1974).

This similarity could be explained by the common origin of these mineral associations: A large part of the fine clay material in the depressions could arrive from the eroded soils of the limestone hills. Some minor differences in the proportions of clay components between the upland and lowland soils could be explained by some further transformation of minerals in the water-saturated environments of the latter. In particular,

we attribute the higher proportion of the smectitic component within the 1.4 nm phase to the degradation of vermiculite (Novikoff et al., 1972). There are other reports of tropical soil catenas with contrasting morphological characteristics but quite uniform clay mineral composition, for example, in coastal Brazil (Pacheco et al., 2018). Pacheco and colleagues explained this phenomenon with erosion/redeposition of pre-weathered material along the hillslope gradient.

If our hypothesis is correct and the depression soils received large amounts of redeposited soil materials, why are these materials not detected morphologically? In particular, why have the fragments of red clayey soil, observed in the thin sections of upland Rendolls, not been found in the lowland Gleysols? We think that the hydromorphic pedogenetic processes within the swampy depression could sweep away morphological features of pedosedimentary materials. Microbial reduction under anaerobic conditions causes translocation of iron from the reduced depletion areas toward oxidation sites where Fe-Mn pedofeatures are formed (Vepraskas et al., 2018). We suppose that, in our case, it results in the decomposition of red ferruginous pigment of pedosediments and concentration of Fe and Mn hydroxides in the nodules observed in the thin sections. This redistribution of iron could also affect the orientation pattern of clay particles. Undifferentiated b-fabric, which we observed in the red soil fragments in the upland profiles, is due to the presence of tiny ferruginous grains which prevent the orientation of platy clay mineral particles. When this ferruginous component is removed due to reduction in the hydromorphic soils of the depression, clay particles could orient and produce striated b-fabric. The main factor of clay particle orientation in the soils is the shear stress related to swelling pressure (Stoops & Mees, 2018). Parallel-oriented clay particles occupy less space than randomly oriented; thus, they are aligned along the planes of sharing, producing striae. We suppose that presence of smectites with high swelling capacity should increase shear stress effects in the studied hydromorphic soils and support development of striated b-fabric. As a result, the set of morphological features of soil mass is deeply transformed, being affected by redoximorphic processes, whereas composition of silicate clay minerals suffers only minor changes and permits us to trace the pedosedimentary origin of the material.

The most intriguing pedogenetic phenomenon in the depression is the presence of abundant neoformed gypsum crystals in some profiles. Gypsum is a moderately soluble component. Thus, gypsiferous soils are common predominantly in the (semi)arid regions where evapotranspiration exceeds precipitation, leaching processes are restricted, or upward transport of dissolved sulfates in the soil profile takes place (Casby-Horton et al., 2015; IUSS Working Group WRB, 2015; Sposito et al., 2008). There are previous findings of neoformed gypsum in the soils of the Maya lowlands, particularly in the pedosedimentary sequences of the coastal

lowlands in Belize (Beach et al., 2006; Krause et al., 2019; Luzzadder-Beach et al., 2012; Pohl et al., 1996). These authors all explain abundant precipitation of sulfates together with carbonates by the same mechanism: evaporation of highly mineralized groundwater that ascended in the Late Holocene due to the sea level rise.

The soils surrounding the site of Budsilhá are formed under a perhumid tropical climate, thus neoformed gypsum is in apparent discordance with the environmental setting. The precipitation here is two to three times higher than further north in the Yucatan peninsula, and thus should produce strong dissolution effect in the surface soil horizons. For this reason, the evaporation mechanism is improbable even in the lowland profiles saturated with groundwater.

Our first idea was that gypsum is a relict feature related to more arid phases in the past. Dry periods occurring throughout the late Holocene in the Maya region are inferred from different proxies: lacustrine (Hodell et al., 2005; Leyden et al., 1996; Torrescano-Valle & Islebe, 2015), speleological (Medina-Elizade et al., 2010; Webster et al., 2007), and marine (Haug et al., 2003). The hypothesis of a drought (or series of droughts) as the main cause of the decline of southern Classic Maya communities has become dominant during the last decades. Thus, we were tempted to interpret the gypsum accumulations as a legacy of ancient droughts, especially taking into account that in the regional lacustrine records, gypsum presence in lake sediment cores is presented as a reliable indicator of aridity (Brenner et al., 2003). Nevertheless, micromorphological observations cast doubt on this hypothesis. If gypsum crystals were inherited from a past environment, in disequilibrium with present-day soil conditions, we would expect some signs of their decomposition: surface dissolution features like etching pits, phantom voids, and so forth (Poch et al., 2018). However, such features were never observed in the gypsum of the wetland soils surrounding Budsilhá. On the contrary, the crystals look fresh and complete even in the A horizon, indicating their recent development.

In the framework of the relict feature version, we should also consider the possibility of the ancient anthropogenic origin of gypsum. Gypsiferous soils have been reported in archaeological contexts where gypsum was derived from ancient construction materials (Golyeva et al., 2018). The archaeological and pedological observations in the wetlands of Busiljá do not support this version. Ancient anthropic activities there are restricted to digging of the drainage canals, no traces of construction or settlement development are found there, and very few artifacts are clearly redeposited. Macroand micromorphological studies revealed only neoformed gypsum crystals, and no traces of gypseous construction materials were found.

We argue that redoximorphic processes could be responsible for the Ca sulfate precipitation in the hydromorphic

soils of the depression. The initial source of sulfur could be dissolved groundwater sulfate; however, in the reduction conditions of wetland soil, it could be transformed into sulfide. Iron from the ferruginous pigment of the red soil pedosediments is also reduced (as discussed above), and thus conditions for iron sulfide precipitation (so-called acidvolatile sulfides and more stable pyrite) appear (Chesworth et al., 2008). Precipitation of sulfides limits sulfur mobility and detains its further migration with groundwater discharge. When groundwater level lowers temporally in slightly elevated parts of wetland, oxidizing conditions make sulfate formation possible again as the result of sulfide oxidation. In the absence of carbonates, acid sulfate soils develop as a result of sulfide oxidation process (Chesworth et al., 2008). However, in our case, sulfate further reacts with the abundant calcium bicarbonate dissolved in the groundwater (provided by the limestone karstification in the surrounding hills). This interaction produces gypsum and neutralizes acidity (Fanning et al., 2002).

This scenario may explain the unexpected variations in the ionic composition of the groundwater within the Busiljá swampy lowland. Indeed, we found substantial difference between the soil water from the slightly elevated part (Gypsic Endoaquepts profiles), where the most abundant anion is sulfate, and that from the lower center of depression (profile Typic Endoaquepts 1), dominated by bicarbonate—despite the fact that both belong to the same continuous groundwater body. We suppose that, only in the periodically aerated elevated part, sulfide oxidation and sulfate formation take place. The latter further reacts with the dissolved bicarbonate, consuming it and generating calcium sulfate; after reaching saturation, it precipitates as gypsum. In the permanently water-saturated central part of the depression, reduced conditions are permanent, sulfate does not form, and hydrogen carbonate remains dominant anion.

The process of gypsum synthesis at the expense of sulfide oxidation in presence of calcium (bi)carbonate is the second most important pathway of formation of this mineral in the soils and continental sediments apart from evaporative precipitation. It is interesting that the shape of gypsum crystals depends on their origin: sulfide oxidation produces predominantly elongated and tabular morphology (as in the studied case!), whereas very common lenticular shapes are generated by the evaporation in arid environments (Mees & Stoops, 2018). The oxidative synthesis of gypsum process is well studied in coastal wetlands (Poch et al., 2009) but is also known in the inland hydromorphic geosystems (Lamontagne et al., 2006); it is frequently also found in the artificial soils on sulfidic mine waste ameliorated with carbonates (Fanning et al., 2002).

Concerning the Maya region, Beach et al. (2008, p. 327) considered the possibility of neoformation of gypsum due to pyrite oxidation unlikely in the lowlands of Belize, but

without discussing this possibility in detail. On the other hand, Leonard et al. (2019) found pyrite—possible precursor for gypsum—in the carbonateous wetland soil-sediment sequences in the north of Yucatán Peninsula. We hypothesize that neoformation of gypsum due to the sulfide oxidation in presence of calcium (bi)carbonate could be a widespread process in the wetland and possibly also in the lacustrine land-scapes of the Maya lowlands, where karstified limestone is the most common geological subsoil material.

If our hypothesis is valid, it will have important implications for paleoecological interpretations of gypsum when it is found in the soils and sediments of the region. In lacustrine sequences, abundance of gypsum (frequently estimated by measuring the sulfur content) is usually judged as an indicator of higher evaporation rates in relation to precipitation and thus seen as a reliable indicator for aridization (Brenner et al., 2003). This interpretation supposes the evaporative origin of gypsum and does not consider the possibility of its formation due to sulfide oxidation. However, if the latter is true, the paleoclimatic interpretation of this component is quite ambiguous because oxidative synthesis of gypsum could also take place under humid climate, as shown above. Anyway, at present, our version of gypsum neoformation is far from being strictly proven; further research is needed to check this hypothesis. In particular, a thorough search for sulfides—the supposed precursor of gypsum—should be undertaken in the deeper horizons of the wetland soils of Busiljá.

Apparently, the presence of neoformed gypsum does not limit biological productivity of the wetland soils. Being a neutral salt with relatively low solubility, it does not affect chemical soil quality. Gypseous horizons could have a negative effect on soil physical properties in case of their cementation (Sposito et al., 2008), although this is not the case in the studied wetland soils. At present, this area has abundant grass vegetation and is used as a pasture. The soils could be cultivated after drainage, and the presence of artificial canals in the area indicates that these soils could form the main agricultural domain of the Classic Maya soilscape. Cultivable plants in these contexts could include a variety of annuals, such as the milpa triumvirate (maize, beans, and squash) or root crops such as manioc (Manihot esculenta) and edible cocoyams (Xanthosoma spp.); commodity and tithe crops such as cotton (Gossypium spp.); leafy plants such as chaya (Cnidoscolus chayamayansa McVaugh); and shrubby fruit plants such as more shallow-rooted nance or annatto (Horseman, 2022). It is likely that taller trees with deeper root systems, such as copal (Protium copal Schltdl. & Cham.) or breadnut (Brosimum alicastrum Swartz) trees, would suffer in periods of higher groundwater levels, even where artificial drainage was employed.

Even with taphonomic conditions that hindered preservation and limited sampling capacity, we see the local

consumption of expected domesticates by residents at the ancient site of Budsilhá. However, the samples taken from the units in the likely agricultural area (Op. 5B) yielded no agricultural products, instead presenting a wide suite of wild and/or non-domesticated plants. These plants may represent the fallowing period of an agricultural cycle. The presence of expected domesticates such as maize, chile peppers, and nance fruits in trash deposits and construction fills demonstrate that Budsilhá residents were making use of some other portion of the landscape to grow these plant foods or were gaining food products in trade. These cultivation areas are likely located in the artificially drained flat lowlands undergoing continuous managed successional cropping, yielding a variety of economic plants dependent on the succession phase of the zone (Morell-Hart et al., 2023). The importance of the lowland agricultural domain should have especially increased during the Classic period when the population (especially urban) grew, whereas upland soil resources had already been largely destroyed by human-induced erosion, as discussed above.

5 | CONCLUSIONS

The studied catenas in the mountainous karstic landscape of Busiljá, Chiapas, show a particular pedogenesis that differs from what is expected of the soil cover in both the tropics and in the karstic geosystems. This phenomenon is in part related to the semicontinuous anthropic occupation of the area. Four primary conclusions are drawn from this study:

- The rendzic-type soils (of shallow profile and high humus content) are not incipient soils but instead are highly eroded. This erosion has occurred primarily through the anthropic activities in the upper part of the terrain that have been taking place in the area for the past 2000 years.
- 2. The soils in the lower parts of the terrain present abundant pedosediments that have been affected and modified by gleyic processes. The relationship between the upper and lower soils is not easily recognizable in the profiles but the clay mineralogy and the micromorphology shed some light on the matter.
- 3. The appearance of neoformed gypsum, in the lower parts of the terrain, is proposed to be of recent formation and not related to the archaeological occupation. This is likely the result of reductomorphic processes and is related to the presence of the water table which contains dissolved hydrocarbonates.
- 4. The distribution of the anthropic activities is closely related to location on the geoform. In the upper parts of the terrain, there is a higher concentration of architectural structures, along the slopes there are terraces that could serve both as agricultural and living spaces, and the lower

parts of the terrain seem to have been reserved for agricultural purposes with some modifications to moderate seasonal overabundance of water.

The soil development and ancient Maya land use in the area were closely intertwined with the geoform and the presence of anthropic activities. Ancient inhabitants clearly designated particular areas for architecture, agriculture, and other activities. However, these inhabitants were necessarily attentive to the pre-existing affordances and limitations of the same areas, such as soil fertility, relatively flat areas for construction, and location in regard to other occupants of the landscape. Over time, transformations to the landscape—transformations some of these ancient inhabitants engendered—could have led to new affordances. Given the soil history now documented in and around Budsilhá, we see new limitations brought on by the erosion of rich soils from agricultural areas, and the overall degeneration of previously reliable upland agricultural zones.

AUTHOR CONTRIBUTIONS

P. Garcia-Ramirez: Data curation; formal analysis; investigation; visualization; writing—original draft; writing review and editing. K. Guillén: Formal analysis; investigation. S. Sedov: Formal analysis; funding acquisition; investigation; writing-original draft; writing-review and editing. C. Golden: Formal analysis; funding acquisition; investigation; visualization; writing—review and editing. S. Morell-Hart: Formal analysis; funding acquisition; investigation; visualization; writing—original draft; writing review and editing. A. Scherer: Formal analysis; funding acquisition; investigation; visualization; writing—review and editing. T. Pi: Formal analysis; investigation; visualization; writing—original draft; writing—review and editing. E. Solleiro-Rebolledo: Funding acquisition; investigation. **H. Dine**: Formal analysis; investigation. **Y. Rivera**: Formal analysis; investigation; visualization.

ACKNOWLEDGMENTS

Research was supported by the Alphawood Foundation of Chicago, the Hitz Foundation, the National Science Foundation (BCS-1917671), the Social Sciences and Humanities Research Council of Canada (435-2019-0837), Brandeis University, Brown University, and McMaster University. We are grateful to the Consejo de Arqueología and the Instituto Nacional de Antropología e Historia for the permission to conduct the archaeological aspects of this work, and our thanks to the local communities whose permission and participation makes this field research possible. This research was partly covered by the Consejo Nacional de Humanidades, Ciencia y Tecnología (CONAHCYT) through the project (CF682138) La infraestructura urbana como indicador de la génesis y desarrollo de la ciudad Maya Clásica: el caso de Palenque,

Chiapas. We acknowledge the financial support given by the projects Programa de Apoyo a Proyectos de Investigación e Innovación Tecnológica PAPIIT-DGAPA, projects IN108622 and IN105819. We thank Jaime Díaz-Ortega for his support during the field work and thin sections' preparation.

CONFLICT OF INTEREST STATEMENT

The authors declare no conflicts of interest.

ORCID

P. García-Ramírez https://orcid.org/0009-0006-7654-6394

C. Golden https://orcid.org/0000-0003-0371-4247
S. Morell-Hart https://orcid.org/0000-0003-1866-8714
H. Dine https://orcid.org/0000-0002-0500-7362

REFERENCES

- Barnhisel, R. I., & Bertsch, P. M. (1989). Chlorites and hydroxy-interlayered vermiculite and smectite. In J. B. Dixon, & S. B. Weed (Eds.), *Minerals in soil environments* (Vol. 1, 2nd ed., pp. 729–788). SSSA. https://doi.org/10.2136/sssabookser1.2ed.c15
- Bautista, F., Palacio-Aponte, G., Quintana, P., & Zinck, J. A. (2011). Spatial distribution and development of soils in tropical karst areas from the Peninsula of Yucatan, Mexico. *Geomorphology*, *135*(3), 308–321. https://doi.org/10.1016/j.geomorph.2011.02.014
- Bautista-Zuñiga, F., Estrada-Medina, H., Jiménez-Osornio, J. J. M., & González-Iturbe, J. A. (2004). Relación entre el relieve y unidades de suelo en zonas cársticas de Yucatán. *Terra Latinoamericana*, 22(3), 243–254.
- Beach, T. (1998a). Soil catenas, tropical deforestation, and ancient and contemporary soil erosion in the Petén, Guatemala. *Physical Geography*, 19(5), 378–405. https://doi.org/10.1080/02723646.1998. 10642657
- Beach, T. (1998b). Soil constraints on northwest Yucatán, Mexico: Pedoarchaeology and Maya subsistence at Chunchucmil. *Geoarchaeology*, *13*(8), 759–791. https://doi.org/10.1002/(SICI)1520-6548(199812)13:8(759::AID-GEA1)3.0.CO;2-B
- Beach, T., Dunning, N., Luzzadder-Beach, S., Cook, D. E., & Lohse, J. (2006). Impacts of the ancient Maya on soils and soil erosion in the central Maya Lowlands. *Catena*, 65(2), 166–178. https://doi.org/10.1016/j.catena.2005.11.007
- Beach, T., Luzzadder-Beach, S., Cook, D., Krause, S., Doyle, C., Eshleman, S., Wells, G., Dunning, N., Brennan, M. L., Brokaw, N., Cortes-Rincon, M., Hammond, G., Terry, R., Trein, D., & Ward, S. (2018). Stability and instability on Maya Lowlands tropical hillslope soils. *Geomorphology*, 305, 185–208. https://doi.org/10.1016/j. geomorph.2017.07.027
- Beach, T., Luzzadder-Beach, S., Dunning, N., & Cook, D. (2008). Human and natural impacts on fluvial and karst depressions of the Maya Lowlands. *Geomorphology*, *101*(1), 308–331. https://doi.org/10.1016/j.geomorph.2008.05.019
- Beach, T., Luzzadder-Beach, S., Krause, S., Guderjan, T., Valdez, F., Fernandez-Diaz, J. C., Eshleman, S., & Doyle, C. (2019). Ancient Maya wetland fields revealed under tropical forest canopy from laser scanning and multiproxy evidence. *Proceedings of the National Academy of Sciences*, 116(43), 21469–21477. https://doi.org/10.1073/pnas.1910553116

- Brenner, M., Hodell, D., Curtis, J., Rosenmeier, M., Anselmetti, F., & Ariztegui, D. (2003). Paleolimnological approaches for inferring past climate change in the Maya region: Recent advances and methodological limitations. In A. Gómez-Pompa, M. Allen, S. L. Fedick, & J. J. Jiménez-Osornio (Eds.), *The lowland Maya area: Three millennia at the human-wildland interface* (pp. 45–76). Food Products Press.
- Cabadas-Baez, H. V., Solleiro, E., Sedov, S., Pi, T., & Alcalá, J. R. (2010a). The complex genesis of red soils in Peninsula de Yucatan, Mexico: Mineralogical, micromorphological and geochemical proxies. *Eurasian Soil Science*, 43, 1439–1457. https://doi.org/10.1134/S1064229310130041
- Cabadas-Báez, H., Solleiro-Rebolledo, E., Sedov, S., Pi-Puig, T., & Gama-Castro, J. (2010b). Pedosediments of karstic sinkholes in the eolianites of NE Yucatán: A record of Late Quaternary soil development, geomorphic processes and landscape stability. *Geomorphology*, 122(3), 323–337. https://doi.org/10.1016/j.geomorph.2010.03.002
- Casby-Horton, S., Herrero, J., & Rolong, N. A. (2015). Gypsum soils—
 Their morphology, classification, function, and landscapes. In D.
 L. Sparks (Ed.), Advances in agronomy (Vol. 130, pp. 231–290).
 Academic Press. https://doi.org/10.1016/bs.agron.2014.10.002
- Chávez-Herrerías, A. (2023). El uso de espacio doméstico externo en dos unidades habitacionales del Maya Clásico de la región de Palenque [Bachelor's thesis, ENAH]. CDMX.
- Chesworth, W., Spaargaren, O., Hadas, A., Groenevelt, P. H., Otero, X. L., Ferreira, T. O., Vidal, P., Macías, F., & Chesworth, W. (2008). Thionic or sulfidic soils. In W. Chesworth (Ed.), *Encyclopedia of soil science* (pp. 777–781). Springer. https://doi.org/10.1007/978-1-4020-3995-9_597
- CONAGUA. (2020). Normales climatológicas por Estado. Estaciones Ixcan, Yaquintela y El Rosario. https://smn.conagua.gob.mx/es/ informacion-climatologica-por-estado?estado=chis
- Darwin, C. (1881). The formation of vegetable mould through the action of worms: With observations on their habits. John Murray.
- Dine, H. (2018b). Budsilhá: Operacion 5B: Investigaciones en la Zona Pantanosa. In A. Scherer, & C. Golden (Eds.), Proyecto Arqueologico Buslilja-Chocolja: Informe de la Novena Temporada de Campo Presentado (pp. 47–57). INAH.
- Dixon, J. B. (1989). Kaolin and serpentine group minerals. In J. B. Dixon, & S. B. Weed (Eds.), *Minerals in soil environments* (Vol. 1, 2nd ed., pp. 467–525). SSSA. https://doi.org/10.2136/sssabookser1.2ed.c10
- Douglas, L. A., Dixon, J. B., & Weed, S. B. (1989). Vermiculites. In J. B. Dixon, & S. B. Weed (Eds.), *Minerals in soil environments* (Vol. 1, 2nd ed., pp. 635–674). SSSA. https://doi.org/10.2136/sssabookser1. 2ed.c13
- Duchaufour, P. (1982). Pedology: Pedogenesis and classification. Springer. https://doi.org/10.1007/978-94-011-6003-2
- Dunning, N. P., Luzzadder-Beach, S., Beach, T., Jones, J. G., Scarborough, V., & Culbert, T. P. (2002). Arising from the bajos: The evolution of a neotropical landscape and the rise of Maya civilization. *Annals of the Association of American Geographers*, 92(2), 267–283. https://doi.org/10.1111/1467-8306.00290
- Durn, G. (2003). Terra rossa in the Mediterranean region: Parent materials, composition and origin. *Geologia Croatica*, 56(1), 83–100. https://doi.org/10.4154/GC.2003.06
- Durn, G., Ottner, F., & Slovenec, D. (1999). Mineralogical and geochemical indicators of the polygenetic nature of terra rossa in Istria, Croatia. *Geoderma*, 91(1), 125–150. https://doi.org/10.1016/S0016-7061(98)00130-X

- Espinasa-Pereña, R. (1990). *Propuesta de clasificación del Karst de la República Mexicana* [Bachelor's thesis, UNAM]. UNAM Repository. http://132.248.9.195/pmig2017/0143123/Index.html
- Fanning, D. S., Rabenhorst, M. C., Burch, S. N., Islam, K. R., & Tangren, S. A. (2002). Sulfides and sulfates. In J. B. Dixon, & D. G. Schulze (Eds.), Soil mineralogy with environmental applications (Vol. 7, pp. 229–260). SSSA. https://doi.org/10.2136/sssabookser7.c7
- Fedick, S. L. (1996). The managed mosaic: Ancient Maya agriculture and resource use. University of Utah Press.
- Fedick, S. L., De Lourdes Flores Delgadillo, M., Sedov, S., Rebolledo, E. S., & Mayorga, S. P. (2008). Adaptation of Maya homegardens by "container gardening" in limestone bedrock cavities. *Journal of Eth-nobiology*, 28(2), 290–304. https://doi.org/10.2993/0278-0771-28.2. 290
- Fernández, F. G., Johnson, K. D., Terry, R. E., Nelson, S., & Webster, D. (2005). Soil resources of the ancient Maya at Piedras Negras, Guatemala. Soil Science Society of America Journal, 69(6), 2020–2032. https://doi.org/10.2136/sssaj2004.0306
- Flores, L., & Alcalá, R. (2010). Manual de procedimientos analíticos. Instituto de Geología, UNAM.
- Flores-Delgadillo, L., Fedick, S. L., Solleiro-Rebolledo, E., Palacios-Mayorga, S., Ortega-Larrocea, P., Sedov, S., & Osuna-Ceja, E. (2011). A sustainable system of a traditional precision agriculture in a Maya homegarden: Soil quality aspects. *Soil & Tillage Research*, 113(2), 112–120. https://doi.org/10.1016/j.still.2011.03.001
- Golden, C., Scherer, A., Schroder, W., Vella, C., & Recinos, A. R. (2020).
 Decentralizing the economies of the Maya West. In C. Golden, A. Scherer, W. Schroder, C. Vella, & A. R. Recinos (Eds.), *The real business of ancient Maya economies* (pp. 403–417). University Press of Florida. https://doi.org/10.5744/florida/9780813066295.003.0023
- Golden, C., Scherer, A. K., Schroder, W., Murtha, T., Morell-Hart, S., Fernandez Diaz, J. C., Jiménez Álvarez, S. D. P., Alcover Firpi, O., Agostini, M., Bazarsky, A., Clark, M., Kollias, G. V., Matsumoto, M., Roche Recinos, A., Schnell, J., & Whitlock, B. (2021). Airborne lidar survey, density-based clustering, and ancient maya settlement in the Upper Usumacinta River region of Mexico and Guatemala. *Remote* Sensing, 13(20), 4109. https://doi.org/10.3390/rs13204109
- Golyeva, A., Khokhlova, O., Lebedeva, M., Shcherbakov, N., & Shuteleva, I. (2018). Micromorphological and chemical features of soils as evidence of bronze age ancient anthropogenic impact (Late Bronze Age Muradymovo settlement, Ural region, Russia). Geosciences, 8(9), 313. https://doi.org/10.3390/geosciences8090313
- Haug, G. H., Günther, D., Peterson, L. C., Sigman, D. M., Hughen, K. A., & Aeschlimann, B. (2003). Climate and the collapse of Maya civilization. *Science*, 299(5613), 1731–1735. https://doi.org/10.1126/science.1080444
- Hodell, D. A., Brenner, M., & Curtis, J. H. (2005). Terminal Classic drought in the northern Maya lowlands inferred from multiple sediment cores in Lake Chichancanab (Mexico). *Quater-nary Science Reviews*, 24(12), 1413–1427. https://doi.org/10.1016/j. quascirev.2004.10.013
- Horseman, G. (2022). Suitability models of Ancient Maya agriculture in the Upper Usumacinta River basin of Mexico and Guatemala [Bachelor's thesis, McMaster University].
- Houston, S. D., & Inomata, T. (2009). The classic Maya. Cambridge University Press.
- INEGI. (1984a). Conjunto de datos vectoriales Geológicos serie
 I. Tenosique (Carta Geológica E15-9). Instituto Nacional de

- Estadística y Geografía. https://www.inegi.org.mx/app/biblioteca/ficha.html?upc=702825236632
- INEGI. (1984b). Conjunto de datos vectoriales Geológicos serie I. Las Margaritas (Carta Geológica E15-12). Instituto Nacional de Estadística y Geografía. https://www.inegi.org.mx/app/biblioteca/ ficha.html?upc=702825236625
- INEGI. (2007a). Conjuntos de Datos Vectorial Edafológico. Escala 1:250 000 Serie II Continuo Nacional Tenosique (Carta Edafológica E15-9). Instituto Nacional de Estadística y Geografía. https://www. inegi.org.mx/app/biblioteca/ficha.html?upc=702825235406
- INEGI. (2007b). Conjuntos de Datos Vectorial Edafológico. Escala 1:250 000 Serie II Continuo Nacional Las Margaritas (Carta edafológica E 15-12, D15-3). Instituto Nacional de Estadística y Geografía. https://www.inegi.org.mx/app/biblioteca/ficha.html? upc=702825235321
- INEGI. (2016). Conjunto de Datos Vectoriales de Uso de Suelo y Vegetación. Escala 1:250000, serie VI (Capa Unión). Instituto Nacional de Estadística y Geografía.
- IUSS Working Group WRB. (2015). World Reference Base for soil resources 2014, update 2015. International soil classification system for naming soils and creating legends for soil maps (World Soil Resources Reports No. 106). FAO.
- Johnson, K. D., Terry, R. E., Jackson, M. W., & Golden, C. (2007).
 Ancient soil resources of the Usumacinta River Region, Guatemala.
 Journal of Archaeological Science, 34(7), 1117–1129. https://doi.org/10.1016/j.jas.2006.10.004
- Kantor, W., & Schwertmann, U. (1974). Mineralogy and genesis of clays in red-black soil toposequences on basic igneous rocks in Kenya. *Journal of Soil Science*, 25(1), 67–78. https://doi.org/10.1111/j.1365-2389.1974.tb01104.x
- Kokalj, Ž., & Somrak, M. (2019). Why not a single image? Combining visualizations to facilitate fieldwork and on-screen mapping. *Remote Sensing*, 11(7), 747. https://doi.org/10.3390/rs11070747
- Krause, S., Beach, T., Luzzadder-Beach, S., Cook, D., Islebe, G., Palacios-Fest, M. R., Eshleman, S., Doyle, C., & Guderjan, T. H. (2019).
 Wetland geomorphology and paleoecology near Akab Muclil, Rio Bravo floodplain of the Belize coastal plain. *Geomorphology*, 331, 146–159. https://doi.org/10.1016/j.geomorph.2018.10.015
- Krause, S., Beach, T. P., Luzzadder-Beach, S., Cook, D., Bozarth, S. R., Valdez, F., & Guderjan, T. H. (2021). Tropical wetland persistence through the Anthropocene: Multiproxy reconstruction of environmental change in a Maya agroecosystem. *Anthropocene*, 34, 100284. https://doi.org/10.1016/j.ancene.2021.100284
- Lamontagne, S., Hicks, W. S., Fitzpatrick, R. W., Rogers, S., Lamontagne, S., Hicks, W. S., Fitzpatrick, R. W., & Rogers, S. (2006). Sulfidic materials in dryland river wetlands. *Marine & Freshwater Research*, 57(8), 775–788. https://doi.org/10.1071/MF06057
- Leonard, D., Sedov, S., Solleiro-Rebolledo, E., Fedick, S. L., & Díaz, J. (2019). Ancient Mayan use of hidden soilscapes in the Yalahau wetlands, northern Quintana Roo, Mexico. *Boletín de La Sociedad Geológica Mexicana*, 71(1), 93–119. https://doi.org/10.18268/BSGM2019v71n1a6
- Leyden, B. W., Brenner, M., Whitmore, T., Curtis, J. H., Piperno, D. R.,
 & Dahlin, B. H. (1996). A record of long- and short-term climatic variation from northwest Yucatan: Cenote San Jose Chulchaca. In S.
 L. Fedick (Ed.), *The managed mosaic: Ancient Maya agriculture and resource use* (pp. 30–50). University of Utah Press.
- Liendo, R., Solleiro-Rebolledo, E., Solis-Castillo, B., Sedov, S., & Ortiz-Pérez, A. (2014). 7 Population dynamics and its relation to ancient

- landscapes in the northwestern Maya lowlands: Evaluating resilience and vulnerability. *Archaeological Papers of the American Anthropological Association*, 24(1), 84–100. https://doi.org/10.1111/apaa. 12031
- Luzzadder-Beach, S., Beach, T. P., & Dunning, N. P. (2012). Wetland fields as mirrors of drought and the Maya abandonment. *Proceedings* of the National Academy of Sciences, 109(10), 3646–3651. https://doi. org/10.1073/pnas.1114919109
- Luzzadder-Beach, S., Beach, T. P., & Dunning, N. P. (2020). Wetland farming and the early Anthropocene: Globally upscaling from the Maya Lowlands with LiDAR and multiproxy verification. *Annals of the American Association of Geographers*, 111(3), 795–807. https://doi.org/10.1080/24694452.2020.1820310
- Maler, T. (1903). Researches in the central portion of the Usumatsintla Valley: Reports of explorations for the museum—Part second. Memoirs 2(2). Peabody Museum of American Archaeology and Ethnology, Harvard University.
- Martin, S. (2020). *Ancient Maya politics: A political anthropology of the classic period 150–900 CE*. Cambridge University Press. https://doi.org/10.1017/9781108676694
- Martin, S., & Grube, N. (2000). Chronicle of the Maya kings and queens:

 Deciphering the dynasties of the ancient Maya. Thames & Hudson.
- Medina-Elizalde, M., Burns, S. J., Lea, D. W., Asmerom, Y., von Gunten, L., Polyak, V., Vuille, M., & Karmalkar, A. (2010). High resolution stalagmite climate record from the Yucatán Peninsula spanning the Maya terminal classic period. *Earth & Planetary Science Letters*, 298(1), 255–262. https://doi.org/10.1016/j.epsl.2010. 08.016
- Mees, F., & Stoops, G. (2018). Sulphidic and sulphuric materials. In G. Stoops, V. Marcelino, & F. Mees (Eds.), *Interpretation of micro-morphological features of soils and regoliths* (2nd ed., pp. 347–376). Elsevier. https://doi.org/10.1016/B978-0-444-63522-8.00013-9
- Merino, E., & Banerjee, A. (2008). Terra rossa genesis, implications for karst, and eolian dust: A geodynamic thread. *The Journal of Geology*, 116(1), 62–75. https://doi.org/10.1086/524675
- Moore, D. M., & Reynolds, R. C. (1997). X-ray diffraction and the identification and analysis of clay minerals (2nd ed.). Oxford University Press.
- Morell-Hart, S. (2018). *Processing and analyzing sediment samples for phytoliths*. McMaster Paleoethnobotanical Research Facility.
- Morell-Hart, S., Dussol, L., & Fedick, S. L. (2023). Agriculture in the ancient Maya Lowlands (part 1): Paleoethnobotanical residues and new perspectives on plant management. *Journal of Archaeological Research*, *31*(4), 561–615. https://doi.org/10.1007/s10814-022-09180-w
- Novikoff, A., Tsawlassou, G., Gac, J.-Y., Bourgeat, F., & Tardy, Y. (1972). Altération des biotites dans les arènes des pays tempérés, tropicaux et équatoriaux. *Sciences Géologiques, bulletins et mémoires*, 25(4), 287–305. https://doi.org/10.3406/sgeol.1972.1421
- Pacheco, A. A., Ker, J. C., Schaefer, C. E. G. R., Fontes, M. P. F., Andrade, F. V., Martins, E. D. S., & Oliveira, F. S. D. (2018). Mineralogy, micromorphology, and genesis of soils with varying drainage along a hillslope on granitic rocks of the Atlantic Forest Biome, Brazil. Revista Brasileira de Ciência Do Solo, 42, e0170291. https:// doi.org/10.1590/18069657rbcs20170291
- Poch, R. M., Artieda, O., & Lebedeva, M. (2018). Gypsic features. In G. Stoops, V. Marcelino, & F. Mees (Eds.), *Interpretation of micro-morphological features of soils and regoliths* (2nd ed., pp. 259–287). Elsevier. https://doi.org/10.1016/B978-0-444-63522-8.00010-3

- Poch, R. M., Thomas, B. P., Fitzpatrick, R. W., & Merry, R. H. (2009). Micromorphological evidence for mineral weathering pathways in a coastal acid sulfate soil sequence with Mediterranean-type climate, South Australia. Soil Research, 47(4), 403–422. https://doi.org/10. 1071/SR07015
- Pohl, M. D., Pope, K. O., Jones, J. G., Jacob, J. S., Piperno, D. R., deFrance, S. D., Lentz, D. L., Gifford, J. A., Danforth, M. E., & Josserand, J. K. (1996). Early agriculture in the Maya Lowlands. *Latin American Antiquity*, 7(4), 355–372. https://doi.org/10.2307/972264
- Priori, S., Costantini, E. A. C., Capezzuoli, E., Protano, G., Hilgers, A., Sauer, D., & Sandrelli, F. (2008). Pedostratigraphy of Terra Rossa and Quaternary geological evolution of a lacustrine limestone plateau in central Italy. *Journal of Plant Nutrition and Soil Science*, 171(4), 509–523. https://doi.org/10.1002/jpln.200700012
- Roche Recinos, A. (2021). Regional production and exchange of stone tools in the Maya polity of Piedras Negras, Guatemala [Doctoral dissertation, Brown University]. Brown Digital Repository. https://repository.library.brown.edu/studio/item/bdr:vqjaf2pw/
- Scherer, A. K., & Golden, C. W. (Eds.). (2012). Revisiting Maler's Usumacinta: Recent archaeological investigations in Chiapas, Mexico. Precolumbia Mesoweb Press.
- Scherer, A. K., & Golden, C. (Eds.). (2018). Informe de la novena temporada de investigación presentado ante el consejo de arqueología del Instituto Nacional de Antropología e Historia. Proyecto arqueológico Busiljá-Chocoljá.
- Scherer, A. K., Golden, C., Guzmán-López, P., & Davenport, B. (2012). Budsilhá: Investigaciones en el Grupo Principal. In A. K. Scherer, C. Golden, & J. Dobereiner (Eds.), Proyecto Arqueologico Buslilja-Chocolja: Informe de la Tercera Temporada de Campo Presentado (pp.10–60). INAH.
- Sedov, S., Solleiro-Rebolledo, E., Fedick, S. L., Pi-Puig, T., Vallejo-Gómez, E., & Flores-Delgadillo, M., & de, L. (2008). Micromorphology of a soil catena in Yucatán: Pedogenesis and geomorphological processes in a tropical karst landscape. In S. Kapur, A. Mermut, & G. Stoops (Eds.), New trends in soil micromorphology (pp. 19–37). Springer. https://doi.org/10.1007/978-3-540-79134-8_3
- Sedov, S., Rivera-Uria, M. Y., Ibarra-Arzave, G., García-Ramírez, P., Solleiro-Rebolledo, E., Cabadas-Báez, H. V., Valera-Fernández, D., Díaz-Ortega, J., Guillén-Domínguez, K. A., Moreno-Roso, S. de J., Fedick, S. L., Leonard, D., Golden, C., Morell-Hart, S., & Liendo-Stuardo, R. R. (2023). Soil toposequences, soil erosion, and ancient Maya land use adaptations to pedodiversity in the tropical karstic landscapes of southern Mexico. Frontiers in Earth Science, 11.
- SGM. (2006a). Carta Geológico-Minera. Tenosique E15-9. Chiapas, Tabasco y Campeche. Servicio Geológico Mexicano.
- SGM. (2006b). Carta Geológico-Minera. Las Margaritas E15-12 D15-3. Chiapas. Servicio Geológico Mexicano.
- Soil Survey Staff. (2022). Keys to soil taxonomy (13th ed.). USDA-NRCS.
- Solís-Castillo, B., Golyeva, A., Sedov, S., Solleiro-Rebolledo, E., & López-Rivera, S. (2015). Phytoliths, stable carbon isotopes and micromorphology of a buried alluvial soil in Southern Mexico: A polychronous record of environmental change during Middle Holocene. *Quaternary International*, 365, 150–158. https://doi.org/10.1016/j.quaint.2014.06.043
- Solís-Castillo, B., Ortiz-Pérez, M. A., & Solleiro-Rebolledo, E. (2014).
 Unidades geomorfológico-ambientales de las Tierras Bajas Mayas de Tabasco-Chiapas en el río Usumacinta: Un registro de los procesos aluviales y pedológicos durante el Cuaternario. Boletín de la

- Sociedad Geológica Mexicana, 66(2), 279–290. https://doi.org/10. 18268/BSGM2014v66n2a5
- Solís-Castillo, B., Solleiro-Rebolledo, E., Sedov, S., Liendo, R., Ortiz-Pérez, M., & López-Rivera, S. (2013). Paleoenvironment and human occupation in the Maya Lowlands of the Usumacinta River, Southern Mexico. *Geoarchaeology*, 28(3), 268–288. https://doi.org/10.1002/gea.21438
- Solleiro, R. E., Terhorst, B., Cabadas, B. H., Sedov, S., Damm, B., Sponholz, B., & Wiesbeck, C. (2015). Influence of Mayan land use on soils and pedosediments in karsic depressions in Yucatan, Mexico. In B. Lucke, R. Bäumle, & M. Schmidt (Eds.), Soils and sediments as archives of environmental change: Geoarchaeology and land-scape change in the subtropics and tropics (Vol. 42). Franconian Geogrphical Society.
- Sposito, G., Chesworth, W., Evans, L. J., Chesworth, W., Spaargaren, O., & Spaargaren, O. (2008). Gypsisols. In W. Chesworth (Ed.), Encyclopedia of soil science (pp. 301–302). Springer. https://doi.org/10.1007/978-1-4020-3995-9 258
- Stoops, G. (2020). Guidelines for analysis and description of soil and regolith thin sections (1st ed.). Wiley. https://doi.org/10.1002/ 9780891189763
- Stoops, G., & Mees, F. (2018). Groundmass composition and fabric. In G. Stoops, V. Marcelino, & F. Mees (Eds.), *Interpretation of micro-morphological features of soils and regoliths* (2nd ed., pp. 73–125). Elsevier. https://doi.org/10.1016/B978-0-444-63522-8.00005-X
- Torrescano-Valle, N., & Islebe, G. A. (2015). Holocene paleoecology, climate history and human influence in the southwestern Yucatan Peninsula. *Review of Palaeobotany & Palynology*, 217, 1–8. https://doi.org/10.1016/j.revpalbo.2015.03.003
- Vepraskas, M. J., Lindbo, D. L., & Stolt, M. H. (2018). Redoximorphic features. In G. Stoops, V. Marcelino, & F. Mees (Eds.), *Interpreta*tion of micromorphological features of soils and regoliths (2nd ed., pp. 425–445). Elsevier. https://doi.org/10.1016/B978-0-444-63522-8.00015-2
- Webster, J. W., Brook, G. A., Railsback, L. B., Cheng, H., Edwards, R. L., Alexander, C., & Reeder, P. P. (2007). Stalagmite evidence from Belize indicating significant droughts at the time of Preclassic Abandonment, the Maya Hiatus, and the Classic Maya collapse. Palaeogeography, Palaeoclimatology, Palaeoecology, 250(1), 1–17. https://doi.org/10.1016/j.palaeo.2007.02.022
- Wojdyr, M. (2010). Fityk: A general-purpose peak fitting program. *Journal of Applied Crystallography*, 43(5–1), 1126–1128. https://doi.org/10.1107/S0021889810030499
- Yaalon, D. H. (1997). Soils in the Mediterranean region: What makes them different? *Catena*, 28(3), 157–169. https://doi.org/10.1016/ S0341-8162(96)00035-5

How to cite this article: García-Ramírez, P., Guillén, K., Sedov, S., Golden, C., Morell-Hart, S., Scherer, A., Pi, T., Solleiro-Rebolledo, E., Dine, H., & Rivera, Y. (2024). Soil development and ancient Maya land use in the tropical karst landscape: Case of Busiljá, Chiapas, México. *Soil Science Society of America Journal*, 1–22. https://doi.org/10.1002/saj2.20723